Modulation of macrophage polarization with surface immobilized bioactive molecules

Alex C. Chen

A dissertation
submitted in partial fulfillment of the
requirements for the degree of

Doctor of Philosophy

University of Washington
2016

Supervisory Committee:
Buddy D. Ratner (Chair)
James D. Bryers
David G. Castner
Lara J. Gamble
Christine K. Luscombe (GSR)

Program Authorized to Offer Degree:
Department of Bioengineering

University of Washington

Abstract

Modulation of macrophage polarization with surface immobilized bioactive molecules

Alex C Chen

Chair of Supervisory Committee:
Professor Buddy D Ratner
Department of Bioengineering

Macrophages are widely recognized as a key cell type in modulating the foreign body response. The manner in which they affect the foreign body response largely depends on their activation state, often referred to as their polarization. The macrophage polarization state lies on a spectrum between two extremes, known as the M1 (inflammatory) polarization and M2 (anti-inflammatory, healing) polarization. It has been demonstrated throughout literature that the polarization state of macrophages depends on many different factors in the cell environment, including the presence of other cells, extra cellular matrix, and soluble factors such as cytokines. In this document, we demonstrate the ability of bioactive molecules that have been immobilized onto a biomaterial surface to modulate the macrophage response. In particular, we support the hypothesis that α-1 acid glycoprotein, as well as Collagen VI in conjunction with α-1 acid glycoprotein, can affect macrophages towards the M2 polarization state, even after immobilization onto a surface. This hypothesis is supported through *in vitro* analysis of cytokines released in macrophage culture media and RT-PCR analysis of genes correlating with M2 polarization. An *in vivo* pilot study of subcutaneous implants with immobilized bioactive molecules also supports our hypothesis through analysis of the foreign body capsule and immunohistochemical staining of macrophages at the implant surface. These data demonstrate that α-1 acid glycoprotein and Collagen VI could potentially be used as a surface coating of medical devices to reduce and modulate the foreign body response, as well as macrophage polarization.

Table of Contents

List of Abbreviations

AGP	α-1 acid glycoprotein
CDI	carbonyl diimidazole
Col6	Collagen VI
DMEM	Dulbecco's modified eagle medium
DNA	deoxyribonucleic acid
DVS	divinyl sulfone
ECM	extracellular matrix
EDA	ethylene diamine
EDC	ethyl(dimethylaminopropyl carbodiimide
ELISA	enzyme linked immunosorbent assay
ESCA	electron spectroscopy for chemical analysis(XPS)
FACS	fluorescence assisted cell sorting
FBC	foreign body capsule
FBGC	foreign body giant cell
FBR	foreign body response
H&E	hematoxylin and eosin
iAGP	immobilized α-1 acid glycoprotein
iCol6	immobilized Collagen VI
IEM	isocyanto ethyl methacrylate
IL	interleukin
IPDI	isophorone diisocyanate
JAK	Janus kinase
LPS	lippopolysaccharide
MCSF	macrophage colony stimulating factor
MECA	mouse endothelial cell antigen
MMR	macrophage mannose receptor
NHS	N-hydroxysuccinimide
NOS2	nitric oxide synthase 2
PBS	phosphate buffered saline
PC	principal component
PCA	principal component analysis
PDMS	poly (dimethylsiloxane)
PE	phycoerythrin
pep1	Badylak peptide sequence 1
pep2	Badylak peptide sequence 2
PerCP	peridinin chlorophyll
PFPE	perfluoro poly ether
pHEMA	poly (2-hydroxyethyl methacrylate)
RF	radiofrequency
RNA	ribonucleic acid

RPMI-1640	Roswell Park Memorial Institute cell culture media
RT	reverse transcription
RT-qPCR	real time quantitative polymerase chain reaction
SDS	sodium dodecyl sulfate
SEM	scanning electron microscopy
STAT	signal transducer and activator of transcription
TBS	tris buffered saline
TEGDMA	triethylene glycol dimethacrylate
TFAA	trifluor acetic anhydride
TFBA	trifluorobutyl amine
THF	tetrahydrofuran
TNF	tumor necrosis factor
ToF-SIMS	time of flight secondary ion mass spectroscopy
TRIS	tris trimethylsiloxy silyl propyl methacrylate
XPS	X-ray photoelectron spectroscopy(ESCA)

List of Figures and Tables

Chapter 1: Introduction and Background

1.1 Motivation

This project was originally started in collaboration with Dr. Karl Böhringer's lab in the UW electrical engineering department. The Böhringer lab is pursuing the creation of microelectronic components that will be used to create a "bionic" contact lens. Our role in this project was to create a contact lens that is compatible with microelectronic devices and can be worn for an extended period of time. Since the project's inception, its goal has become more generalized, aiming to modulate macrophage polarization for any medical application. We hope to surface immobilize bioactive molecules that will reduce inflammation and improve comfort of extended contact lens wear. The bioactive molecules that we investigate include α-1 acid glycoprotein (AGP) and collagen VI (Col6), which have been shown to reduce the inflammatory phenotype of macrophages when they are introduced in solution. We will also investigate the effect of other bioactive molecules such as lipopolysaccharide (LPS) and Interleukin-4 (IL-4), which have been shown to affect macrophage polarization as well.

1.2 Soft contact lenses

1.2.1 Overview

Soft contact lenses were first created in 1970 by Otto Wichterle out of poly-2(hydroxyethyl methacrylate) (pHEMA). pHEMA (Fig. 1-1), because it is a hydrogel, is a material that is highly hydrophilic and resistant to protein adsorption. However, pHEMA does not provide for high oxygen permeability, which is a key property of comfortable and safe contact lenses [1]. To address this problem, more advanced materials have been developed for contact lenses that have much higher oxygen permeability.

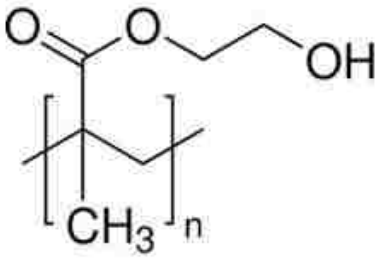

Figure 1-1 Chemical structure of pHEMA.

1.2.2 Contact lens complications

Complications resulting from wear of contact lenses are experienced by approximately 6% of wearers in the United States. These complications can be caused by a variety of factors, including improper care, damaged lenses, predisposing conditions, and pathogens. Two properties that are imperative for comfortable and safe soft contact lenses are oxygen permeability and a hydrophilic surface. If a contact lens does not have high enough oxygen permeability, the cornea will undergo hypoxia, which can result in chronic or acute edema. Low hydrophilicity will lead to the buildup of protein and lipid deposits, which can lead to irritation or more severe complications [2].

1.2.3 Silicone hydrogel materials

To address the issues of hydrophilicity and oxygen permeability, many modern contact lenses are made of silicone hydrogels. Silicone hydrogels have high oxygen diffusivity due to the bulkiness of the siloxane group (–Si(CH3)2–O–) and high chain mobility within the materials. Polydimethylsiloxane (PDMS) is a commonly used siloxane-containing polymer used in silicone hydrogels. Perfluoropolyethers (PFPE) are also often used in silicone hydrogels due to their high oxygen solubility properties. These two kinds of materials together form a material with very high oxygen permeability. In order to increase the hydrophilicity of the silicone hydrogels, co-monomers such as dimethyl acrylamide (DMA) are included in the final polymerization formula.

1.2.4 Extended wear versus short term wear

Of the over 34 million contact lens wearers in the United States, more than 80% of these patients use a daily wear schedule, meaning the contact lenses are applied and removed daily. The majority of these patients would prefer to use an extended wear schedule, involving wearing the lenses overnight, allowing them to reduce handling of the contact lens. However, patients are deterred from extended wear of contact lenses due to discomfort and eye irritation [3]. Extended wear of contact lenses also increases the likelihood of complications developing.

1.3 Macrophages

1.3.1 Overview

Macrophages are phagocytic cells involved in adaptive immunity, pathogen removal, tissue regeneration, and iron homeostasis [4]. In addition, they play an important role in the foreign body response, which includes the response to contact lenses worn on the cornea. The function of macrophages depends on the phenotypic polarization of the cells, which are generally classified as either classically(M1) or alternatively (M2) activated macrophages. The polarization of the macrophages can be triggered by a variety of factors, including cytokines and cell environment.

1.3.2 Origin of macrophages

Macrophages differentiate from circulating peripheral-blood mononuclear cells, and migrate into all tissues in the steady state or in response to inflammation [4]. In the bone marrow, hematopoietic stem cells are stimulated by macrophage colony stimulating factor to become mononuclear cells, which enter the blood stream after maturation.

1.3.3 Classically activated macrophages

The term classically activated, or M1 polarized, has been used to describe macrophages that are present during the cell-mediated immune response. These macrophages are characterized by enhanced microbicidal and tumoricidal capacity, and secretion of pro-inflammatory cytokines, such as IL-1, IL-6, and IL-23 [4,5]. They also phenotypically express nitric oxide synthase 2 (NOS2), interleukin-1 receptor 1 (IL-1R1), and C-C chemokine receptor-7 (CCR-7) markers on their surfaces [6]. M1 polarization can be triggered by bioactive molecules such as interferon-γ(IFN-γ), tumor necrosis factor (TNF), lipopolysaccharides (LPS), and endotoxin. Classically activated macrophages are important to the host defense against pathogens, but the pro-inflammatory cytokines released by them can also be detrimental to the healing process.

1.3.4 Alternatively activated macrophages

Alternatively activated, or M2 polarized, macrophages comprise of several different subpopulations of macrophages that perform different functions from classically activated macrophages. They can be activated by cytokines such as Interleukin-4 (IL-4) and Interleukin-10 (IL-10), as well as glucocorticoids and toll-like receptor ligands, among other factors. They are involved in many functions, including tissue remodeling, scavenging of debris, angiogenesis, and immunoregulation [4]. Alternatively activated macrophages are commonly classified into the three subpopulations of M2a, M2b, and M2c. Each is activated by different triggers, and each have shared and unique characteristics of each other. They commonly secrete cytokines such as IL-10, interleukin-1 receptor A (IL-1RA), and arginase, and phenotypically express macrophage mannose receptor (MMR), Arginase -1 (Arg1), and scavenger receptor-I/II (SR-BI/II) on their surfaces.

1.4 The foreign body reaction (FBR)

1.4.1 Overview

The FBR refers to how living tissue responds to implanted foreign materials, and is an important factor in determining the long-term performance of medical devices. The FBR historically has been the cause of many medical device failures and complications, such as the impaired functionality of glucose sensors and stiffening and pain of breast implants. When a contact lens is worn on the eye, the response of the human body is very similar to that of implanted medical devices. A greater understanding of the biological mechanisms of the FBR will allow the design of improved medical devices and medical care, including a more comfortable contact lens for extended wear.

1.4.2 Progression of FBR

The FBR begins as soon as a foreign material is implanted into the host tissue. Tissue damage triggers native wound healing events, including platelet degranulation, which releases a variety of proteins that attract neutrophils and macrophages to the implant site. The implant surface is quickly coated with adsorbed proteins, which affect cell attachment and signaling. A provisional extracellular matrix forms

around the implant, leading to acute inflammation followed by chronic inflammation, which lasts up to two weeks. Granulation tissue then begins to form at the implant surface, as well as foreign body giant cells (FBGCs), which are the result of multiple macrophages fusing into one multinucleated cell. Eventually, a fibrous capsule composed largely of collagen, forms around the implanted material [7].

1.4.3 Negative effects of the FBR

The FBR is useful in protecting the native tissue from unwanted foreign objects. The fibrous capsule, also referred to as the foreign body capsule (FBC), that forms will isolate the foreign material, effectively creating a barrier between the native tissue and foreign object. However, when the FBC forms around medical devices, they can cause a variety of problems. Monitoring devices, such as diabetes glucose sensors, can be rendered useless because the FBC prevents bodily fluids from reaching the sensors, making detection of analytes impossible [8]. Devices such as pacemakers may also undergo failure due to the oxidizing environment caused by FBGCs, which can damage electronic components [9]. Mechanical moving parts of some implants, such as artificial heart valves, may also undergo hindrance of their performance due to movement restrictions that occur when their components undergo calcification that is the result of the FBR [10]. These are only a few examples of why it is important to better understand the FBR to improve the performance of various medical devices.

1.4.4 Macrophages in the FBR

Macrophages are believed to play a major role in mediating the FBR. After they arrive at the surface of the foreign object, they attempt to degrade and phagocytose the object, as well signal to other cells involved in the FBR. Eventually, they fuse together to form FBGCs in an attempt to envelop the foreign object. The cells recruited to the FBR site by macrophages and FBGCs include fibroblasts and endothelial cells, which begin forming the FBC and blood vessels. The activity of the FBR is believed to be determined by the type of activation of the macrophages involved [8]. With a better understanding of how to control the classical or alternative polarization of macrophages at a foreign body, it may be possible to have a greater control over the resulting FBR and FBC formation.

1.5 Objectives

The goal of this project is to develop a technique to immobilize bioactive molecules that will reduce the M1 inflammatory phenotype of macrophages. In particular, we hope to use cytokines that have been shown to promote the M2 phenotype of macrophages, and to immobilize them onto biocompatible surfaces in order to reduce inflammation for applications such as contact lenses and improve healing for applications such as implanted medical devices.

Hypothesis: Immobilized bioactive molecules will reduce the inflammatory phenotype of macrophages in contact with the modified surface, as well as increase their M2 polarization.

Contact lens substrate fabrication: Fabricate a silicone hydrogel contact lens that is hydrophilic, biocompatible, and oxygen permeable.

Bioactive molecule immobilization: Develop a technique for immobilization of bioactive molecules onto surfaces of medical devices

***In vitro* testing of surface immobilized bioactive molecules:** Perform *in vitro* analysis of the macrophage polarizing capabilities of immobilized bioactive molecules.

***In vivo* testing of surface immobilized bioactive molecules:** Perform *in vivo* analysis of the effect of immobilized M2 macrophage polarizing bioactive molecules on the FBR.

Chapter 2: Create a contact lens material substrate material

2.1 Introduction

In order to create a contact lens that is compatible with microelectronic devices and suitable for extended wear, we pursue the development of a silicone hydrogel based lens. The contact lens material we design must have good mechanical properties to protect the electronic components, while still providing the contact lens properties of being transparent, oxygen permeable, and having a high refractive index. Silicone hydrogels provide us with all of these properties, which can be finely tuned with the addition of different monomers.

2.2 Background

2.2.1 Oxygen permeability and silicone hydrogels as a contact lens material

In order to maintain a healthy cornea, contact lenses need to have high oxygen permeability. The oxygen transport properties of a lens is commonly referred to as Dk/t, where Dk is the intrinsic properties of the lens material, expressed in barrer, while t refers to the thickness of the particular lens [1]. A Dk/t value of 87 barrer/mm is required for healthy extended wear of a contact lens [10]. Because water has a Dk of 80, regular hydrogels with high water content are deemed insufficient for extended contact lens wear. Silicone hydrogels, with their incorporated PDMS and PFPE units, have Dk values varying from approximately 100-190 Dk. Because they can be polymerized with hydrophilic monomers, as well as monomers to increase mechanical properties, they are an appropriate material for contact lens development.

2.3 Materials and Methods

2.3.1 Silicone hydrogel components

The silicone hydrogel macromer is composed of four main components: a polydimethylsiloxane (PDMS), a perfluorpolyether (PFPE), isophorone diisocyanate (IPDI), and isocyanatoethyl methacrylate (IEM) (Fig. 2-1). The PDMS used is a dihydroxyl-terminated molecule with an average molecular weight of 600-850 daltons, DMS-C16 (Gelest, Morrisville, PA). DMS-C15, with a molecular weight of 1000 daltons, was also

tested. The PFPE used is a Fomblin ZDOL, also dihydroxyl-terminated, with a molecular weight of 2000 daltons (Solvay Solexis, Orange, TX). IPDI is a cyclic aliphatic compound with two isocyanate groups, and is used as a linker molecule between the PFPE and PDMS molecules. IEM is a molecule with one isocynate group, and is used as an end capping molecule for the silicone hydrogel macromer. Its carbon-carbon double bonds are used in the polymerization process.

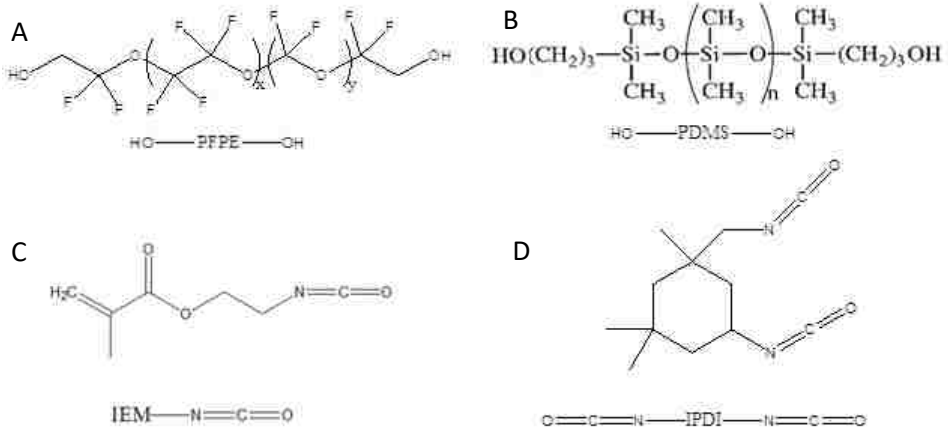

Figure 2-1. Chemical structures and abbreviations of A) Fomblin ZDOL B) di-hydroxypropyl terminated polydimethylsiloxane C) isocyanato ethyl methacrylate and D) isophorone diisocyanate.

2.3.2 Urethane chemistry and silicone hydrogel formulation

The silicone hydrogel formulation is based on a patent by Lynn Winterton [11]. The macromer formation involves reacting the hydroxyl groups on the PDMS and PFPE compounds with the isocynate groups on the IPDI and IEM compounds (Fig. 2-2). The IPDI behaves as a linker molecule by being able to form urethane bonds at both of its isocyanate groups, while IEM only has one isocyanate group available for urethane bonding. The Winterton patent describes a silicone hydrogel macromer that has one molar ratio of PFPE as the center of the macromer, which is reacted with two molar ratio of IPDI. This in turn is reacted with two molar ratio of PDMS, which urethane bonds with the IPDI terminated PFPE. Finally, this product is then reacted with 2 molar ratio of IEM, which end caps the macromer with carbon-carbon double bonds. All urethane bond formations are catalyzed using dibutyltin dilaurate. After formation of the macromer, the macromer was then polymerized with dimethyl acrylamide (DMA) and Tris trimethylsiloxy silyl propyl methacrylate (referred to as Tris), with Darocur 1173 as the catalyst (Fig. 2-3). Polymerization

was done under a UV lamp for 10 minutes. After polymerization, the silicone hydrogel was cleaned three times in a soxhlet extractor, using hexane, methanol, and acetone as solvents. Triethylene glycol dimethacrylate (TEGDMA) was added during the polymerization step to increase mechanical properties of the polymerized silicone hydrogel.

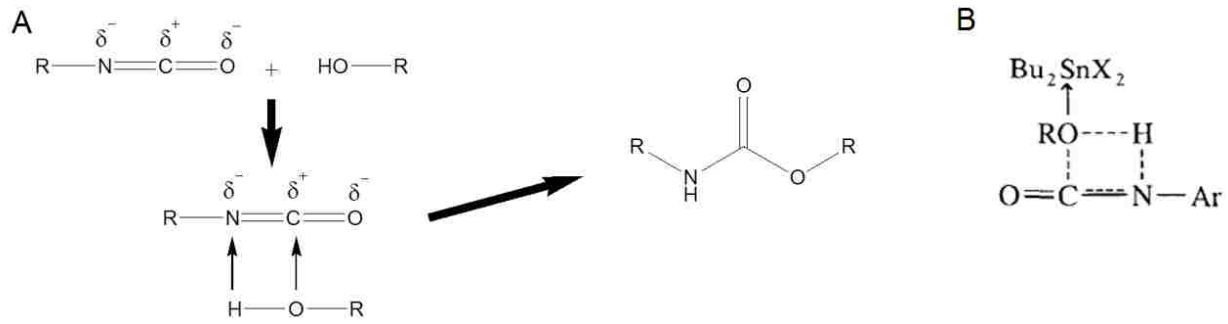

Figure 2-2 Urethane bond chemistry A) Urethane bond formation between isocyanate group and hydroxyl group. B) Catalysis of urethane bond formation by dibutyltin dilaurate.

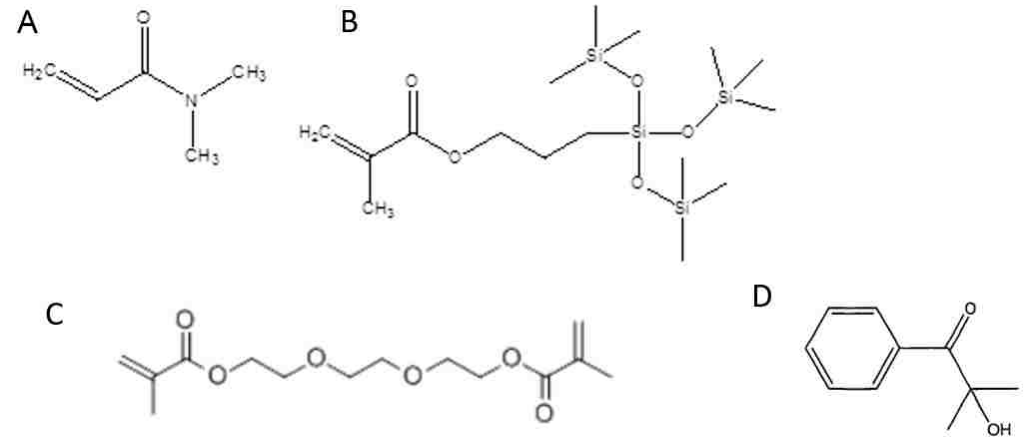

Figure 2-3 Structures of silicone hydrogel co-monomers A) dimethyl acrylamide B) TRIS and C) TEGDMA co-monomers. D) Structure of Darocur 1173 used for catalysis of UV polymerization

2.3.3 Tensile testing to measure silicone hydrogel mechanical properties

Tensile testing was performed on an Instron 5543 Advanced Materials Testing System (Instron, Norwood, MA). Silicone hydrogel samples were cut into dog bone shapes of 5mm width and 2mm thickness. Samples were immersed in a BioPuls water bath with deionized water at 37°C during testing to maintain their water content. Tensile extension was performed at 10mm/min until sample failure.

2.4 Results

2.4.1 Silicone hydrogel formulation

The Winterton formulation was based off of a PFPE with a molecular weight of 1000 amu, but we were only able to obtain Fomblin ZDOL with a molecular weight of 2000 amu. This resulted in a macromer formulation that was cloudy and opaque. It is believed that this lack of transparency was due to microphase separation of the macromer segments, which causes anisotropic regions within the polymer structure. The many micro-scale anisotropic regions cause the diffraction of light that passes through the polymer, resulting in a non-transparent material [12].

To address this problem, we fabricated a modified composition that uses the PDMS molecule as the center molecule of the macromer, resulting in a 1:2 ratio of PDMS to PFPE. One molar ratio of PDMS was first reacted with 2 molar ratio of IPDI, which was in turn reacted with 2 molar ratio of PFPE and then 2 molar ratio of IEM (Fig. 2-4). This macromer was transparent in its liquid form, and also showed transparency after polymerization.

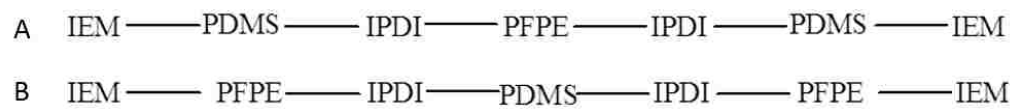

Figure 2-4 Silicone hydrogel macromer structures for A) original macromer formulation using Fomblin ZDOL 1000 and B) modified formulation to incorporate Fomblin ZDOL 2000

2.4.2 Silicone hydrogel polymerization

Initial UV polymerization of the silicone hydrogel macromer was unsuccessful, resulting in no solidification of the material. It was hypothesized that polymerization was being inhibited by butylated hydroxytoluene (BHT) that was present in the macromer mix (Fig. 2-5). IEM is stored with BHT in order to prevent the IEM from polymerizing. To remove the BHT from the macromer mix, the IEM was first purified by filtering through a syringe filled with DHR-4 beads (Scientific Polymer, Ontario, NY). Silicone hydrogel macromer formed with the purified IEM polymerized under UV light using the composition shown in Table 2-1.

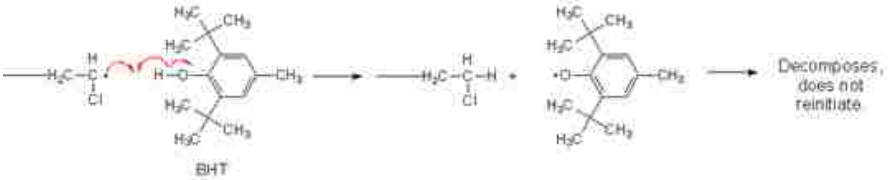

Figure 2-5 BHT inhibition of polymerization by scavenging of free radicals

Macromer	4.09 g	41%
TRIS	1.64 g	16%
DMA	2.46 g	25%
EtOH	1.76 g	17%
Darocur	1 drop	<0.5%
TEGDMA	0.1 g	1%

Table 2-1. Formulation for silicone hydrogel polymerization mix

2.4.3 Silicone hydrogel tensile tests

Tensile testing of polymerized silicone hydrogel samples showed that addition of TEGDMA increased the Young's elastic modulus of the polymer by approximately two fold. Silicone hydrogels synthesized from the DMS-C16 showed a slightly higher elastic modulus than silicone hydrogels synthesized from DMS-C15 (Table 2-2). Commercial contact lenses show an elastic modulus ranging from 0.3 to 1.8 MPa [13].

	Elastic modulus
DMS-C15	0.27 MPa
DMS-C16	0.39 MPa
DMS-C16+1%TEGDMA	0.82 MPa

Table 2-2 Tensile testing results for silicone hydrogels formulated from both DMS-C15 and DMS-C16 PDMS variants.

2.5 Discussion

By modifying the silicone hydrogel macromer composition found in the Winterton patent, we were able to synthesize a macromer that is transparent and polymerizable. This macromer was easily polymerized with the addition of different co-monomers to improve its mechanical properties, which can be tuned to the desired Young's modulus by adding the co-monomers in different concentrations. The material is hydrophilic and should provide adequate oxygen diffusion properties for contact lens applications due to its incorporation of PDMS and PFPE.

Chapter 3: Immobilization of bioactive molecules

3.1 Introduction

We believe that macrophage modulating bioactive molecules (particularly α-1 acid glycoprotein and Collagen VI) can reduce the M1 inflammatory phenotype of macrophages, even after immobilization of these molecules onto a surface. To immobilize these bioactive molecules, we developed a plasma deposition process of pHEMA to provide a hydrophilic surface that has hydroxyl groups that are available for covalent bonding of molecules to the surface. These hydroxyl groups can be activated using different chemistries and incubated with our molecules of interest for covalent immobilization.

3.2 Background

3.2.1 Plasma deposition of pHEMA

Radiofrequency (RF) plasma deposition of pHEMA is a substrate coating technique that provides several advantages. By changing the conditions of the RF plasma, the substrate can either be etched or coated with a desired polymer. The etching condition provides a way of cleaning the substrate, which then can be ionically activated to provide good adhesion to the polymer overlayer. The process is conformal and repeatable, providing a uniform overlayer of the deposited polymer, and is independent of the substrate surface chemistry. This means the process can be developed for one substrate material, and easily applied to different substrate materials and applications. In addition, the plasma deposition process crosslinks the HEMA monomer into a mechanically strong pHEMA overlayer without any further polymerization techniques needed [14].

3.3 Materials and Methods

3.3.1 Plasma deposition of pHEMA

A polymer overlayer generated from HEMA was deposited onto the silicone hydrogel surface under vacuum (~5-10 mTorr) in a tubular glass plasma chamber. Ophthalmological grade HEMA (Polysciences, Warrington, PA) was degassed by freezing in liquid nitrogen, under vacuum, and then thawing until minimal bubbles showed while thawing. Samples were first etched in argon plasma at 20 watts, under

250mTorr of argon gas pressure for 5 minutes, to remove any surface contamination on the samples. The chamber is then pumped down to remove argon and etching byproducts. A methane layer was first deposited to improve polymer adhesion to the substrate. Methane was introduced into the chamber at 1.5sccm, at 150mTorr of pressure. Methane was then deposited at 80 watts for 5 minutes. Next, a pHEMA layer was deposited onto the surface. The HEMA flask was kept at 65°C in a water bath. HEMA, which vaporizes under low pressure and heating, is introduced into the plasma chamber and allowed to equilibrate at 250mTorr. The HEMA plasma was first treated at 100 watts for 1 minute to ensure good adhesion of the pHEMA layer to the substrate/methane surface, and then deposited and polymerized at 6 watts for 20 minutes. After plasma deposition, the plasma was turned off, and the pHEMA vapor was allowed to quench the surface for 5 minutes at 250mTorr. After deposition, samples were soaked in deionized water for 3 days, changing water each day, to observe any delamination of the pHEMA overlayer from the soaking procedure.

3.3.2 Ellipsometry to measure the thickness of plasma deposited pHEMA layers

The plasma deposited pHEMA overlayer thickness was measured using a M-2000 Spectroscopic Ellipsometer (Woollam, Lincoln, NE). Ellipsometry is an optical technique that uses the amplitude ratio and phase difference of light that is reflected from the substrate surface. The overlayer thickness and material determines the effect on amplitude and phase, which can be modeled in the computer software to calculate the overlayer thickness. The ellipsometer was run at 55, 65, and 75° angles, from 200-1700 nm wavelengths [15]. Refractive index of the pHEMA layer was assumed to be 1.5. Modeling was done using the Cauchy model, which assumes the pHEMA is transparent.

3.3.3 Trifluoroacetic anhydride derivatization to assess functionality of hydroxyl groups

Trifluoroacetic anhydride (TFAA) (Sigma-Aldrich, St. Louis, MO) was reacted with pHEMA coated substrates in order to determine if the pHEMA overlayer had functional hydroxyl groups. During the plasma deposition process, the plasma ionization will cause the ionization and possibly removal of hydroxyl groups from the pHEMA. RF plasma power was lowered during the deposition step in order to

minimize the loss of hydroxyl groups from the deposited pHEMA. TFAA was introduced into a large glass tube in which the pHEMA coated substrates were placed. The tube was then heated to 37°C, allowing the TFAA to vaporize and react with the pHEMA coatings, for 15 minutes. This process is referred to TFAA derivatization. The samples were then rinsed in deionized water, dried, and analyzed using XPS for an increase in fluorine content [16].

3.3.4 Synthesized Badylak peptides

Two peptide sequences obtained from the Badylak lab (McGowan Institute, Pittsburg) were custom synthesized and purchased from GenScript (Piscataway, NJ). These peptide sequences have shown chemoattractant effects for macrophages, and are derived from digested porcine extracellular matrix [56]. Peptide sequences were synthesized (>95% purity) with an acetic acid counterion and were aliquoted to 10mg vials. Peptides were solubilized in deionized water for ToF-SIMS studies or HEPES buffer for immobilization studies. These peptides are used for testing of the covalent immobilization techniques, as well as studied to see if they have effects on macrophage polarization.

Badylak peptide sequence 1 (pep1): IAGVGGEKSGGF

Badylak peptide sequence 2 (pep2): GPVGPSGPPGK

3.3.5 Carbonyl diimidazole (CDI) and divinyl sulfone (DVS) peptide immobilization

CDI and DVS chemistries were used to covalently bond peptide and protein sequences to the pHEMA surfaces. Both of these compounds have two active groups that can form covalent bonds with hydroxyl groups and/or primary amine groups, acting as a linker molecule between the pHEMA surface and peptides.

For CDI immobilization (Fig. 3-1), samples were first dried by rinsing in 1,4-dioxane three times. Samples were then incubated with 100mM CDI (Sigma-Aldrich, St. Louis, MO) in dioxane solution at 40°C for 2.5 hours. CDI activated samples were then rinsed three times in dioxane to remove any excess CDI, and then incubated in 100uM peptide solutions in sodium bicarbonate/sodium carbonate buffer at pH 10.2 for 24 hours at 40°C [17].

DVS (Sigma) immobilization (Fig. 3-2) was performed on pHEMA samples that were first lyophilized overnight and then soaked in tetrahydrofuran (THF) for 30 minutes. The samples were then activated in DVS by incubation in a solution of 1.1mM potassium tert-butoxide (Sigma) and 1.6mM DVS in 10mL of THF for 3 hours on a shaker at room temperature. After activation, the samples were rinsed five times in fresh THF to remove excess DVS, and then dried in low vacuum to remove the THF solution. Samples were then incubated in 2.5mM peptide solutions made with HEPES buffer (Sigma), adjusted to pH of 8.0 using tris(hydroxymethyl) aminomethane (Fisher Scientific, Fair Lawn, NJ) [18].

Peptide immobilized samples were rinsed three times in 1% sodium dodecyl sulfate (SDS) solution to remove any nonspecifically adsorbed peptides, and then rinsed five times in deionized water to remove residual SDS [19]. Samples were then analyzed in XPS and ToF-SIMS to confirm peptide immobilization.

Trifluorobutylamine (TFBA, Oakwood Chemical, West Columbia, SC) and porcine angiotensinogen (Sigma) were used to test the peptide immobilization techniques. TFBA is a small molecule with an amine group available for our immobilization techniques, and has three fluorine atoms that are easily detected by XPS. Angiotensinogen is a 14 amino acid peptide sequence produced by the liver that is similar in size to the peptide sequences from the Badylak lab.

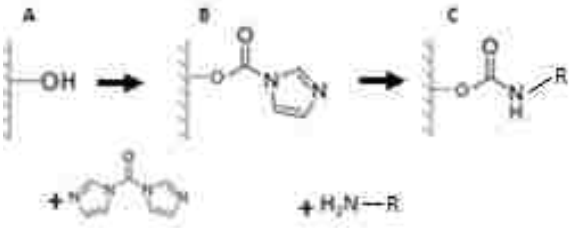

Figure 3-1. Carbonyl diimidazole immobilization reaction

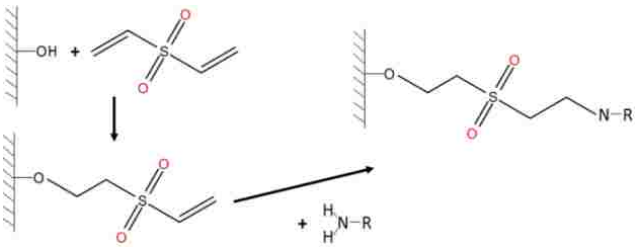

Figure 3-2. Divinyl sulfone immobilization reaction

3.3.6 EDC-NHS immobilization

A carbodiimide coupling technique was also implemented to immobilize peptide sequences. Ethyl(dimethylaminopropyl carbodiimide (EDC) is used in conjunction with N-hydroxysuccinimide (NHS) to covalently bond amine groups (Fig. 3-3). EDC-NHS is often used to immobilize organic molecules such as heparin and collagen [20]. This technique was used in conjunction with CDI immobilization and ethylene diamine (EDA) to provide functional amine groups on the pHEMA surface.

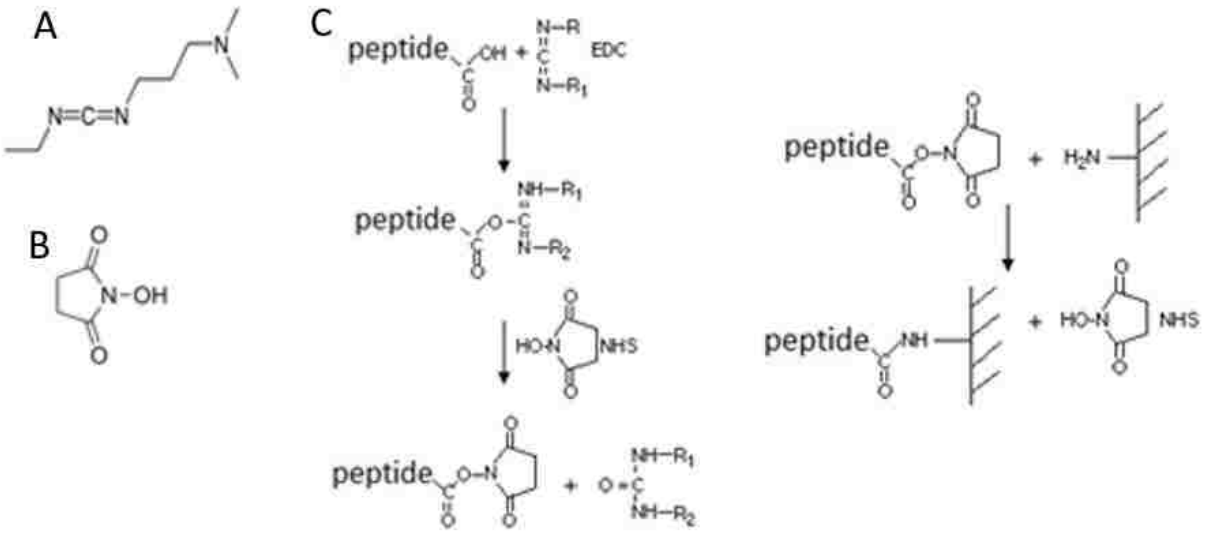

Figure 3-3. Structure of A) EDC and B) NHS. C) The EDC-NHS immobilization reaction.

3.3.7 X-ray photoelectron spectroscopy (XPS) for surface analysis

XPS, also referred to as electron spectroscopy for chemical analysis (ESCA), is a surface analysis technique that allows quantitative measurement of elemental composition at the sample surface. Typically, the probing depth of XPS is about 8nm, and can be accurate up to the parts per thousand range. Briefly, XPS uses an X-ray source to irradiate the sample surface, giving electrons enough kinetic energy to escape the sample surface. Escaped electrons are collected into an electron energy analyzer and electron detector, allowing a plot to be made of the number of electrons collected (y-axis) against the binding energy of the electrons collected (x-axis). The energy of the electrons collected corresponds to

the electron configuration of the electrons within the atoms. XPS must be performed under ultra-high vacuum to ensure electrons are able to travel from the surface to the collector [21]. XPS analysis was done using an S-Probe (Surface Sciences Instruments), while data analysis was performed with ESCA Hawk analysis software.

3.3.8 Time of Flight-Secondary Ion Mass Spectroscopy (ToF-SIMS) analysis

ToF-SIMS is considered to be the most sensitive surface analysis technique that allows for the detection of ions sputtered off of the sample surface. Briefly, a primary ion beam is accelerated and focused onto the sample surface. This ion beam can be generated from a variety of sources, including noble gases or even ionized molecules (C_{60}^{+}). This ion beam causes fragmentation and ionization of the sample surface, creating secondary ions, which are accelerated by an electric field before being collected by the time of flight mass analyzer. The electric field accelerates secondary ions sputtered by the ion beam so they have the same kinetic energy and travel at different speeds according to their mass. The time of flight mass analyzer is thus able to determine the mass of secondary ions that are collected relative to their travel time to the analyzer, represented by peaks indicating the intensity of each particular secondary ion. This technique, although not easily used for quantitative analysis, provides a profile of ionic fragments from the surface, allowing for a more detailed profile of the molecular structures at the sample surface [22]. This information allows us to detect the presence of amino acids, and thus peptide sequences, on our sample surfaces. ToF-SIMS analysis of our samples was performed using the TOF.SIMS^5 (ION-TOF, Münster, Germany). Ion sources used include Bismuth 3 and Bismuth 1.

3.4 Results

3.4.1 Plasma deposited pHEMA overlayer analysis

The presence of a pHEMA overlayer after plasma deposition was confirmed using XPS. Silicon chips were used to optimize the pHEMA deposition process. RF power and sample position were changed until we were able to determine the optimal settings for pHEMA adhesion to the substrate, while depositing an overlayer with functional hydroxyl groups. XPS analysis of pHEMA coated silicon chips under optimal

settings showed a surface composition of 52% carbon, 30% oxygen, and 18% silicon. The appearance of silicon in the XPS scans implies that the thickness of the pHEMA layer is less than 8 nm. The ratio of 52:30 for carbon to oxygen is near the pHEMA carbon to oxygen ratio of 2:1, indicating that the deposited layer has intact pHEMA molecules.

Ellipsometric analysis (Fig. 3-4) showed that the plasma deposited pHEMA overlayer on silicon chips was 3.03 ± 0.01 nm in thickness. With a low mean square error (MSE) of 5.66, we can be confident that this measurement is accurate within the defined deviation.

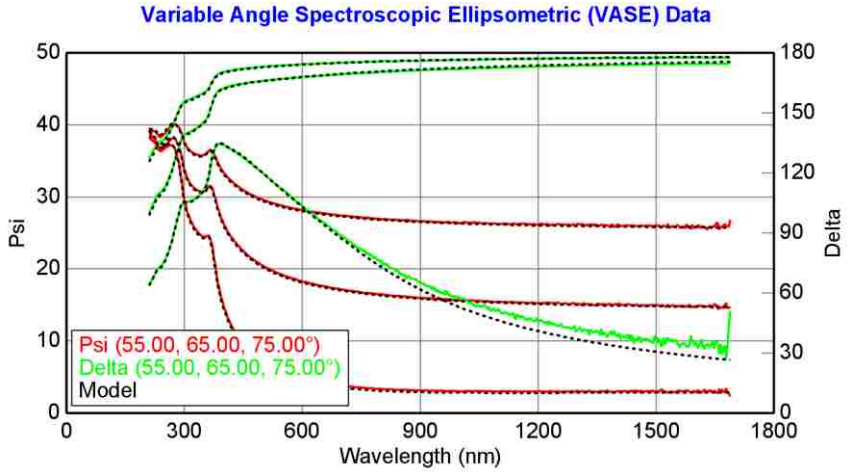

Figure 3-4. Ellipsometry plots of plasma deposited pHEMA on silicon chips using the Cauchy model.

XPS analysis of TFAA derivatized pHEMA surfaces showed 18.3% fluorine content, indicating that there were functional hydroxyl groups on the pHEMA overlayer surface. Pure pHEMA is expected to show ~23% fluorine content after derivatization [23], which is close to the 18.3% analyzed on our plasma deposited surfaces. A high-resolution carbon scan also showed the expected peak corresponding to a carbon bonded to three fluorine atoms (Fig. 3-5).

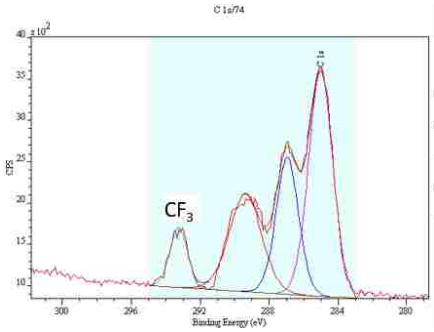

Peak	Binding Energy	Area	Group %
1	285	3285.6	27.94
2	286.738	5201	44.2
3	289.78	2384.2	20.24
4	293.684	899.1	7.62

Figure 3-5. High resolution ESCA carbon scan of TFAA derivatized pHEMA coated silicone chip.

Plasma deposition of pHEMA onto the silicone hydrogel substrate was confirmed via XPS (Table 3-1). This was determined by looking at the surface composition of the substrate. Without the pHEMA overlayer, we see the carbon to oxygen ratio of the silicone hydrogel material is approximately 2.8. After plasma deposition, the carbon to oxygen ratio changes to 2.4. This is because pHEMA has a carbon to oxygen ratio of about 2:1, while the silicone hydrogel material has a much higher carbon to oxygen ratio. In addition, we see that the fluorine content of the pHEMA coated substrate is much lower. This is because there is no fluorine present in pHEMA. Fluorine signal is still detected however, since the probing depth of XPS is greater than the pHEMA overlayer thickness.

	Silicone Hydrogel Only	Silicone Hydrogel with pHEMA
Si2s	5.4±2.1	5.6±0.8
C1s	50.6±2.3	56.4±0.4
N1s	5.0±0.5	4.7±0.8
O1s	18.0±0.5	23.8±0.9
F1s	21.1±0.6	9.5±0.8

Table 3-1. Percentage of surface composition comparing silicone hydrogel and silicone hydrogel with plasma deposited pHEMA.

High resolution carbon scans of the silicone hydrogel surface compared to silicone hydrogel plasma coated with pHEMA was also indicative of the presence of pHEMA (Fig. 3-6). pHEMA coated silicone hydrogel showed much smaller peaks corresponding to carbon atoms bonded to fluorine atoms, which are only present in the silicone hydrogel substrate. This indicates that the pHEMA layer is attenuating the signal from these particular carbon atoms. We expected the nitrogen content of the pHEMA coated silicone hydrogel to be reduced, but it remained around 5%. We believe this may be due to contamination from residual atmospheric nitrogen in the plasma chamber during the deposition process.

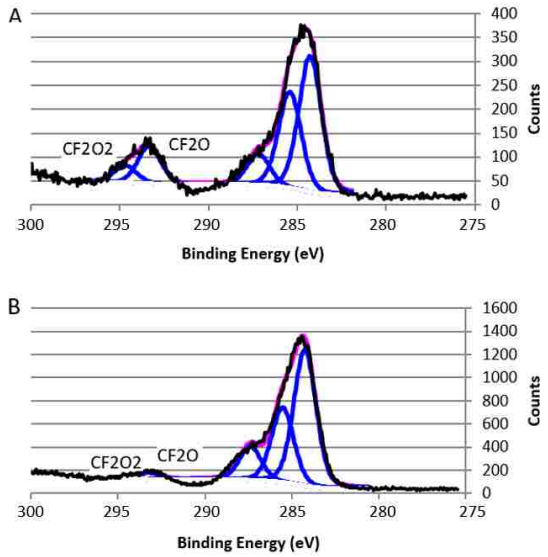

Peak	Binding Energy	Area	Group %
1	284.6	7413	42.459
2	276.278	5299	30.354
3	276.278	1746	9.999
4	276.278	2076	11.89
5	276.278	925	5.298

Peak	Binding Energy	Area	Group %
1	284.6	30964	53.838
2	276.255	17012	29.581
3	276.255	7607	13.227
4	276.255	1450	2.521
5	276.255	478	0.833

Figure 3-6. High resolution carbon scans show different profiles for carbon atoms present in A) uncoated silicone hydrogel and B) plasma pHEMA coated silicone hydrogels. Peaks are number from right to left.

3.4.2 CDI Immobilization testing

CDI immobilization was tested with TFBA, angiotensinogen, and bovine serum albumin (Sigma). 24-hour incubation of CDI activated samples in these test compounds at 100uM in sodium carbonate/sodium bicarbonate buffer at pH 10.2 showed successful immobilization. Immobilization was confirmed using XPS (Table 3-2); nitrogen content of CDI activated samples incubated with test peptides was higher than the nitrogen content of CDI activated samples incubated in pure buffer solution. High resolution nitrogen scans also showed a difference in nitrogen profiles (Fig. 3-7); CDI activated samples without immobilized peptides showed a two-peak nitrogen profile, while samples with immobilized peptides show a one peak nitrogen profile. In addition, samples incubated with TFBA showed an increase of fluorine content at the surface.

	CDI only	CDI with angiotensinogen	CDI with TFBA
Si	1.9	1.9	0.8
C	62.3	64.9	61.2
N	5.2	11.4	5.7
O	25.5	20.2	20.7
F	3.0	1.8	11.4

Table 3-2. Percentage ESCA composition pHEMA coated silicone hydrogel slabs after treatment with CDI only, CDI + angiotensinogen, or CDI + TFBA.

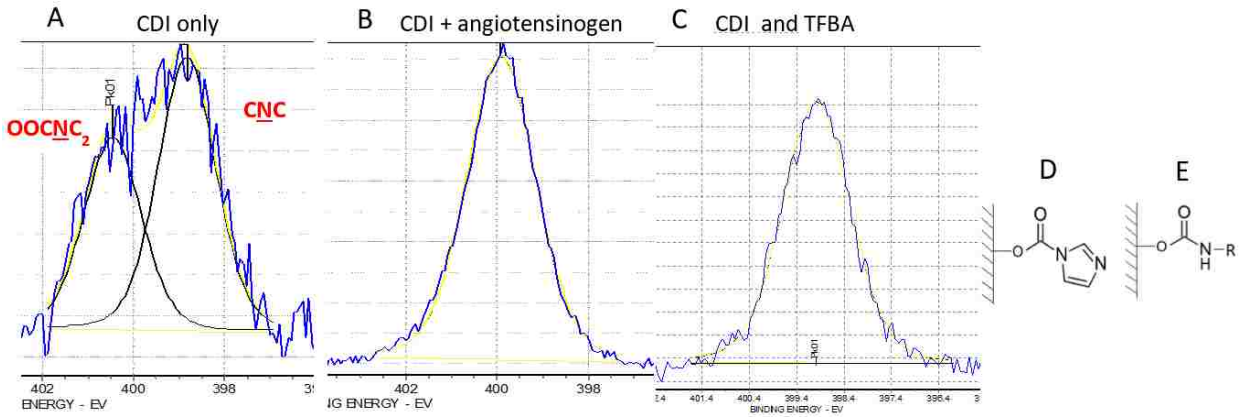

Figure 3-7. ESCA High resolution nitrogen scans of pHEMA coated silicone hydrogel slabs after treatment with A) CDI only B) CDI + angiotensinogen or C) CDI + TFBA. D) Structure of CDI activated hydroxyl group and E) structure of hydroxyl group activated with CDI and then covalently bound to a peptide.

3.4.3 CDI immobilization of Badylak peptides

Badylak peptides, from here on referred to as pep1 and pep2, were incubated with CDI activated pHEMA coated slabs under the same conditions as TFBA and angiotensinogen. XPS analysis showed insignificant increase in nitrogen content at the sample surfaces, as well as no change in high resolution nitrogen profiles. Many attempts were made to optimize the incubation conditions. The buffer pH was varied from pH 7 to pH 11, as well as incubation temperature increased and the use of a hybridizer for thorough mixing during the incubation step. Incubation buffer was also changed; organic solvents dimethylsulfoxide, dioxane and tetrahydrofuran were tested. None of these changes enhanced the immobilization of pep1 and pep2.

3.4.4 EDC-NHS immobilization of peptides

A carbodiimide coupling technique was implemented to test the immobilization of peptide sequences. Ethyl(dimethylaminopropyl carbodiimide (EDC) was used in conjunction with N-hydroxysuccinimide (NHS), ethylene diamine (EDA) and CDI (Fig. 3-8). CDI was first used to activate the pHEMA surfaces for immobilization of EDA, which was performed under the same conditions as the CDI processes as mentioned above. The immobilized EDA provides primary amine groups that will be used in the EDC-

NHS reaction. Peptides were added at 100μM into 0.1M MES buffer with 0.1M EDC and 0.2M NHS. EDA coated samples were then incubated into this reaction solution for 4 hours at room temperature.

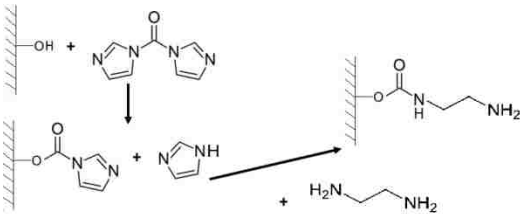

Figure 3-8. CDI immobilization of ethylene diamine to a hydroxyl coated surface.

EDC-NHS immobilization of angiotensinogen as the test peptide showed a slight increase of nitrogen content over EDA coated samples. ToF-SIMS was performed on EDA coated samples and compared to angiotensinogen immobilized samples. Peak analysis showed the presence of amino acid fragments present due to angiotensinogen, while these peaks were not present on EDA coated samples (Fig. 3-9).

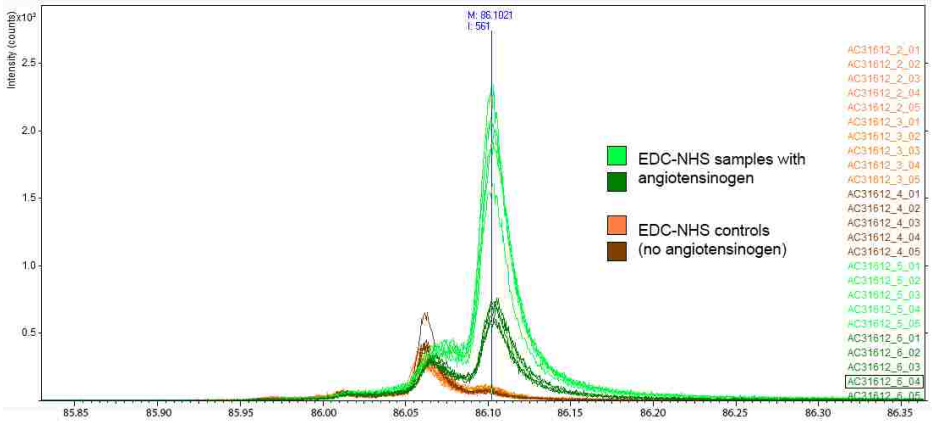

Figure 3-9. Example of a ToF-SIMS peak present in angiotensinogen immobilized samples but not in EDA coated samples, peak of leucine fragment $C_5H_{12}N$ at 86.10

Subsequent EDC-NHS immobilization of Badylak peptides 1 and 2 did not show presence of immobilized peptides.

3.4.5 DVS immobilization of peptides

DVS immobilization proved to be most effective when performed in a hybridizer, typically used for molecular pathology, which provided consistent heating and mixing via a vertically rotating carousel mounted in a small oven. IL-4 was also immobilized onto the DVS surfaces, at an incubation

concentration of only 18.5nM due to its high cost. Because DVS contains no nitrogen, the DVS activated surfaces showed no nitrogen content before incubation with peptides, implying that all nitrogen present during XPS was a result of immobilized peptides (Fig. 3-10).

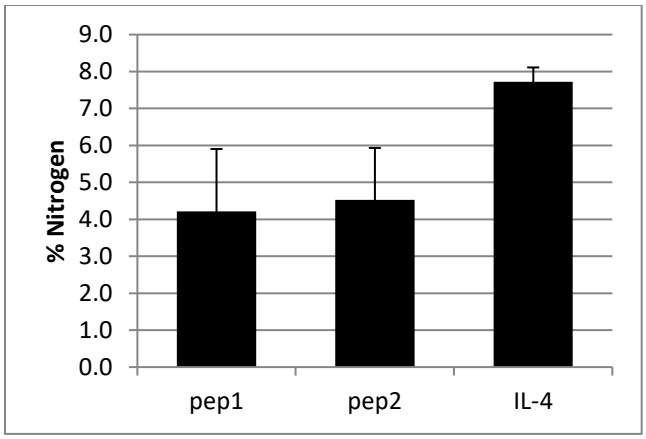

Figure 3-10. Nitrogen content of pHEMA surfaces activated with DVS and incubated with different peptides. DVS activated surfaces with no peptide incubation showed zero nitrogen content.

3.4.6 Relative intensity of nitrogen signal of peptide overlayer on pHEMA substrate

For a uniform overlayer B on a substrate A, the relative intensity I for element X in layer B in proportion to element Y in layer A can be represented by the equation:

$$\frac{I_B}{I_A} = \lambda_X/\lambda_Y \left(e^{\frac{t_B}{\lambda_X sin\theta}} - 1\right) \text{[24]}$$

where λ is the mean free path of electrons from the element of interest within the layer, t is the thickness of the overlayer B, and θ is the incidental angle of the photoelectron source. λ can be calculated using the equation

$$\lambda = \frac{M}{\rho n} E_k/(13.6\ln(E_k) - 17.6 - \frac{1400}{E_k}) \text{[24]}$$

where M is the molecular weight of the repeat unit of the layer, n is the number of valence electrons in the repeat unit, ρ is the density of the layer, and E_k is the kinetic energy of the element. For nitrogen in a layer of pep1, we calculate λ to be 3.13 nm, and for carbon in a layer of pHEMA we calculate λ to be 3.35 nm. Assuming that the immobilized pep1 forms a uniform monolayer at the pHEMA surface, we can approximate the thickness of this layer as the diameter of pep1. This diameter can be estimated using the average density of globular proteins, approximately 0.73cm^3/g [25], which results in a spherical diameter of 1.36 nm. We believe there is no fixed tertiary structure of these peptide sequences, due to their short

length, and believe random bond angles of the sequence resulting in a relatively spherical approximation is appropriate. With an incident angle of 55°, we calculate $I_B/I_A = 0.584$, meaning that the signal intensity of nitrogen in the peptide overlayer will only be 58.4% as intense as the carbon signal intensity in the substrate. With a nitrogen content of approximately 4.2% seen in XPS, we can calculate the actual surface composition of the samples to be 7.2% nitrogen. (Detailed calculations in the Appendix)

3.5 Discussion

Plasma deposition was used to coat the substrate materials with a uniform layer of pHEMA that had hydroxyl groups that were viable for peptide immobilization. Using optimized conditions of the plasma deposition process produced a pHEMA layer that did not delaminate from the substrate surfaces after soaking in deionized water.

CDI and DVS proved able to immobilize TFBA, angiotensinogen, IL-4 and albumin with great consistency. However, immobilization of the Badylak peptides proved to be very inconsistent. Many immobilization conditions were tested, but only DVS immobilization using HEPES pH8 buffer at 45°C in a hybridizer provided consistent immobilization of the Badylak peptides. Even these optimized conditions only showed 4-5% nitrogen content at the substrate surfaces.

The relative intensity of the nitrogen signal from the Badylak peptide overlayer on a pHEMA substrate was calculated to be 58.4% of the relative intensity of the carbon signal from the pHEMA substrate. This is due to the probing depth and angle of the XPS technique, and can explain why we are getting a much lower nitrogen content than we would expect to get from a uniform layer of immobilized peptide (14% nitrogen). However, seeing 7% nitrogen at the surface indicates there is a significant amount of peptide being immobilized, compared to 0% nitrogen with the DVS activated surfaces that were not incubated with peptides.

Chapter 4: *In vitro* analysis of immobilized bioactive molecules on macrophage polarization

4.1 Introduction

M1 and M2 polarized macrophages express different markers on their cell surfaces, as well as secrete different bioactive molecules [26]. Using these markers and molecules, we can assess the polarization of macrophages using a variety of techniques, including fluorescence assisted cell sorting (FACS), real-time polymerase chain reaction (RT-PCR), and enzyme-linked immunosorbent assay (ELISA). Primary bone marrow derived macrophages (BMDMs) isolated from mouse femurs are used for *in vitro* experimentation to see the effect of bioactive molecules on their polarization. In addition, we hope to assess the effect of immobilization on the ability of these molecules to polarize BMDMs.

4.2 Background

4.2.1 Interleukin-4 (IL-4) in macrophage polarity

IL-4 is a cytokine that induces the differentiation of T-cells into Th2 cells [27]. It is also involved in several adaptive immunity roles, while overproduction of IL-4 is associated with the development of allergies. Production of peroxisome proliferator-activated receptor-γ (PPARγ), which is important in reducing inflammation of endothelial cells, is also dependent on the presence IL-4 [28]. IL-4 has been shown to alternatively activate macrophages, which is marked by increased expression of the mannose receptor [29, 8, 46]. IL-4, like many cytokines, signals cells through the JAK-STAT pathway (Fig. 4-1) [30]. Although the IL-4 ligand-receptor complex is readily internalized by cells [31], it is believed the internalization process is not necessary for signaling caused by IL-4. This internalization process of cytokine-receptor complexes is a method of downregulation of the cytokine signal.

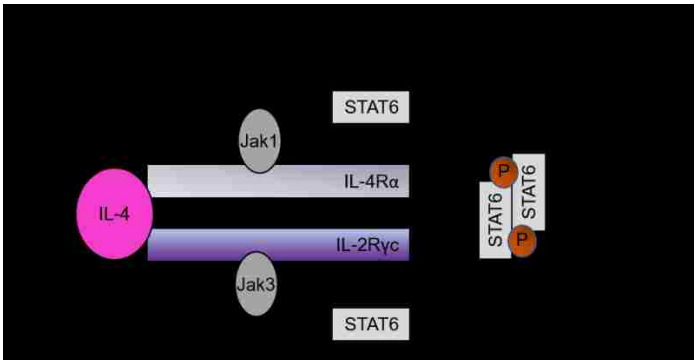

Figure 4-1. The IL-4 transduction pathway.

4.2.2 The NOS2 protein

NOS2 (inducible nitric oxide synthase) is a surface enzyme that produces nitric oxide, which is important in cell signaling. NOS2 also plays a large role in wound healing, affecting angiogenesis, inflammation, and various immune responses [32]. Regulation of NOS2 has been shown to depend on the NF-κB and JAK-STAT pathways [33]. Staining for NOS2 has been shown to be prevalent in macrophages involved in the FBR, where the majority of macrophages stained positive for NOS2 at the site of foreign body inflammation [34]. NOS2 has been shown to be highly expressed in M1 polarized macrophages, and thus was used as one of the markers for M1 polarization of BMDMs [35].

4.2.3 Macrophage Mannose Receptor

Macrophage mannose receptor (MMR) is a transmembrane glycoprotein that is primarily found on macrophages and dendritic cells [36]. It is involved in mediating phagocytosis and endocytosis during the immune response by recognizing complex carbohydrates on glycoproteins [37]. MMR has been shown to be downregulated when macrophages are stimulated with INF-γ, and upregulated when stimulated with IL-4 [40]. Thus, MMR can be considered a marker for M2 macrophage polarization.

4.2.4 Arginase 1

Arginase 1 (Arg1) is an enzyme located primarily in the cytoplasm of hepatic cells that disposes of ammonia. It has a trimeric structure, and is found in nearly all forms of life. It is also expressed in macrophages [38], and is associated with the immune response. It is often used as a marker for M2 polarization, which we will be utilizing in RT-PCR [39, 40].

4.2.5 Interleukin-10

Interleukin-10 (IL-10) is a cytokine involved in the anti-inflammatory response. It is involved in regulation of the JAK-STAT pathway [41], and can block the NF-κB pathway [42]. IL-10 is primarily produced by monocytes [43] and, to a lesser extent, lymphocytes [44]. Expression of IL-10 is typically very low in

unstimulated tissues [45]. However, expression of IL-10 is greatly upregulated in M2 polarized macrophages [46]. IL-10 has also been shown to increase the M2 polarization of macrophages *in vitro* [46]. IL-10 activates the JAK-STAT pathway through the IL-10R1 surface receptor (Fig. 4-2). The IL-10 receptor ligand complex has been shown to be internalized to downregulate the signaling of IL-10. However, when IL-10R1 cannot be internalized, there is prolonged signaling of the JAK-STAT pathway [47, 48]. This is indicative of IL-10 behaving as a signaling molecule solely through its binding with the surface receptor, and does not have to be internalized to have signaling effects.

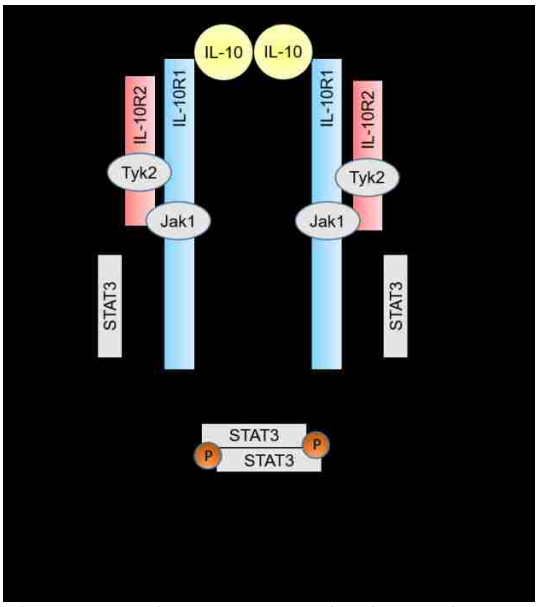

Figure 4-2. The IL-10 transduction pathway.

4.2.6 Tumor Necrosis Factor-α

TNF-α is an adipokine involved in regulating immune cells and inflammation. It also upregulates NF-κB and apoptotic pathways [49]. TNF-α is produced by a variety of cells, including lymphoid cells, mast cells, and endothelial cells. Its production is highly upregulated in M1 polarized macrophages [50].

4.2.7 The JAK-STAT pathway

The JAK-STAT pathway consists of a cell surface receptor, Janus kinase (JAK), and Signal Transducer and Activator of Transcription (STAT) (Fig. 4-3). There are many JAK-STAT pathways present in macrophages, many of which are used by cytokines such as IL-4 and IL-10. JAKs bind to cell surface

receptors, which activate the JAKs when their ligands bind to them. The JAKs phosphorylate tyrosine residues on the receptors to which they are bound, allowing STATs possessing SH2 domains to bind to these phosphotyrosine residues. These STATs form dimers, which then accumulate in the cell nucleus and activate transcription of their target gene. The pathway generally does not require the internalization of the receptor ligand to induce signaling in the cell nucleus.

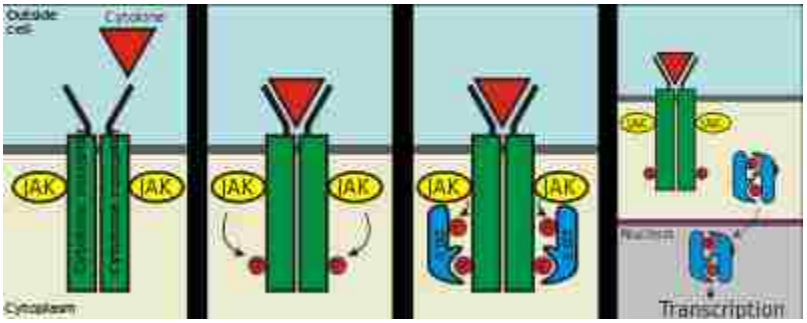

Figure 4-3. The JAK-STAT pathway
(Public domain image from *http://en.wikipedia.org/wiki/JAK-STAT_signaling_pathway*)

4.2.8 α-1 acid glycoprotein

α-1 acid glycoprotein (AGP), also known as orosomucoid, is a glycoprotein that is present in mammalian serum. The exact function of AGP remains unclear, but it has been shown to be associated with various processes, such as binding to lipophilic charged compounds and immunomodulatory effects. AGP is approximately 42 kDa in size, and consists of 45% carbohydrate, with the majority of the amino acid sequence homologous between human, mouse, and rat. It is primarily produced in hepatic cells, but has also been shown to be produced locally by various cells and tissues, including leukocytes, epithelial cells, lungs, and kidneys in response to an acute inflammatory reaction [51]. *In vitro* experiments have shown AGP to upregulate CD163 (an M2 macrophage marker) when introduced to human monocytes in solution [52]. We hope to show that immobilized AGP will also upregulate BMDMs after immobilization to our plasma deposited pHEMA surfaces.

4.2.9 Collagen VI

Collagen VI (Col6) is a protein that is a major component of microfibrils in skeletal muscle. It is typically produced by fibroblasts and muscle cells. Col6 molecules interact to form tetramers, which linearly

aggregate into triple helical structures. These triple helical structures of Col6 are the basis from which microfibrils are formed. [53]. Col6 is involved in modulating macrophage polarization and regeneration in peripheral nerve cells *in vivo*, where mice with no Col6 gene expression had fewer M2 macrophages at the site of nerve injury. Col6 has also been shown to have M2 polarizing effects and chemotactic effects of macrophages *in vitro*. [54]. We hope to observe these M2 polarizing effects of Col6 after it has been immobilized to a biomaterial surface.

4.2.10 Lipopolysaccharides as an M1 agonist

Lipopolysaccharides(LPS), also known as endotoxins, are well documented to be strong M1 polarizing compounds [5, 43]. They are found on the outer membrane of gram-negative bacteria, and consist of an "O antigen" polysaccharide chain bound to an oligosaccharide "core", which is in turn connected to "Lipid A", a disaccharide with multiple fatty acid chains (Fig. 4-4). LPS protects the bacterial membrane from certain chemical attacks, and elicits a strong inflammatory response from animal immune systems [55]. We use LPS as an M1 agonist for controls as well as testing of our experimental techniques.

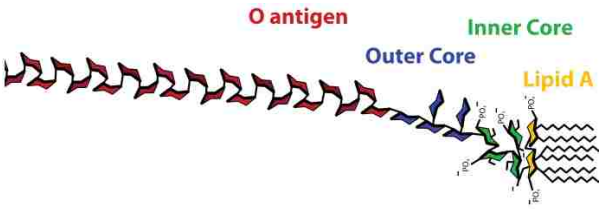

Figure 4-4. The structure of a typical lipopolysaccharide
(Public domain image from https://en.wikipedia.org/wiki/Lipopolysaccharide).

4.2.11 The extracellular matrix and its degradation peptides

The extracellular matrix (ECM) consists of a variety of organic materials, including polysaccharides, proteoglycans, and fibrous proteins. It is defined as being the extracellular part of multicellular tissue structure. It provides support for the tissue structure, and is involved in cell signaling and many other biological processes. [56] The Badylak lab in the University of Pittsburgh, as mentioned previously, has shown that short peptide sequences that are degradation products of the ECM have chemoattractant properties, and are likely involved in regulating the healing process [57]. Some of these peptides are hypothesized to also influence the polarization of macrophages. We will also be testing the degradation

products of porcine urinary bladder matrix (UBM) to see if they will affect the polarization of macrophages in solution and immobilized.

4.3 Materials and Methods

4.3.1 Isolation and expansion of BMDMs

Primary macrophages were collected from mice. Femurs from recently sacrificed mice were harvested and sterilized by soaking in 70% EtOH for 60 seconds. Femurs were then rinsed in RPMI 1640 media, and then the ends of the bones were cut off with surgical scissors. The bones were then flushed with RPMI using a syringe and 25-gauge needle. Marrow cells flushed from the bones were then cultured on non-tissue culture polystyrene plates in RPMI (Gibco, Grand Island, NY), with added fetal bovine serum (RM Bio, Missoula, MO) and penicillin-streptomycin (Gibco) at a density of $5x10^6$ cells per 100mm plate. Macrophage colony stimulating factor (Peprotech, Rocky Hill, NJ) (MCSF) was added at 10ng/mL to stimulate the differentiation of myeloid progenitor cells into macrophages. Non-macrophage cells are unable to adhere to the non-tissue culture treated plates, and were removed during the media change and washing with phosphate buffered saline (PBS) at day 7. Media was added at day 4 of culture (without replacing the old media), and mature BMDMs (Fig. 4-5) were ready for experiments on day 7 [58].

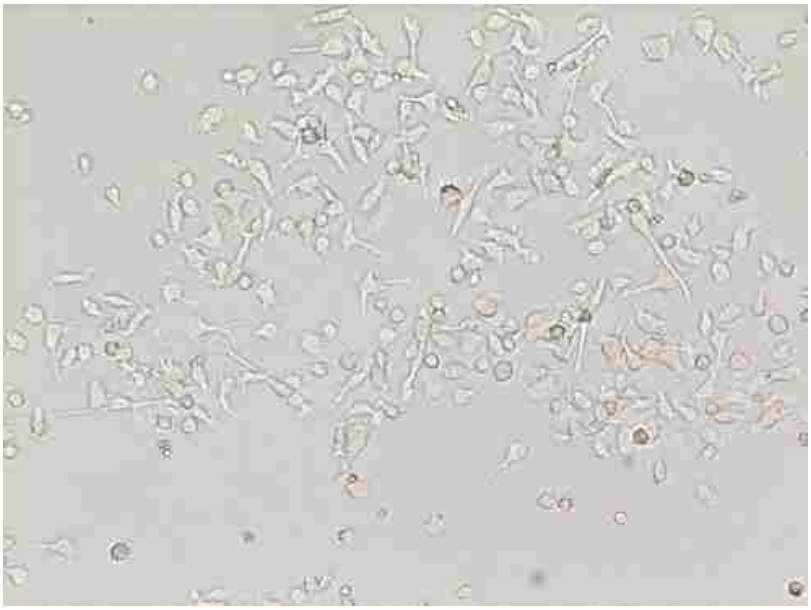

Figure 4-5. BMDMs on day 7, cultured on non-tissue-culture polystyrene

4.3.2 Macrophage polarization by soluble bioactive molecules

LPS and IL-4 were tested in solution to see their effect on macrophage polarization. BMDMs isolated and expanded from mice as described above were cultured in non-tissue culture treated petri dishes. On day 7 of culture, cell media was replaced with fresh media, and bioactive molecules were added to the media. LPS was added at 200 ng/mL, IL-4 was added at 120 ng/mL, and pep1 and pep2 were added at 100mM. Assays were performed at 48 hours after addition of bioactive molecules to assess macrophage polarization.

4.3.3 Immobilization onto glass slides

In order to culture cells on a surface with immobilized bioactive molecules, 10mm glass slides(Ted Pella, Redding, CA) were used due to the fact that CDI and DVS immobilization techniques are incompatible with polystyrene tissue culture plates. 10mm glass slides were first coated with pHEMA via plasma deposition as described above. The surfaces were then activated with CDI solution (as described above), and incubated with LPS (0.05mg in 3mL incubation buffer) or IL-4 (1ug in 3mL incubation buffer) to immobilize them onto the surface. AGP and Col6 were immobilized in the same method, with AGP at 0.3mg/mL and Col6 at 0.125mg/mL. Slides with both Col6+AGP had Col6 and AGP immobilized onto them simultaneously, at 0.0625mg/mL and 0.25mg/mL, respectively.

4.3.4 Fluorescence activated cell sorting (FACS) to determine expression of surface markers

FACS is a method of flow cytometry that utilizes antibodies attached with fluorescent dyes to sort cells that are expressing different surface markers [59]. In this method, primary antibodies for cell surface markers of interest are incubated with the sample cells. These primary (1°) antibodies can have fluorescent dyes such as peridinin chlorophyll (PerCP) or phycoerythrin (PE) attached to them. If 1°antibodies with no dyes are used, the cell samples can be incubated again with a secondary (2°) antibody that has an affinity for the primary antibodies (referred to as indirect staining). These 2° antibodies would have a fluorescent dye attached.

For indirect staining of cells for FACS, $0.5x10^6$ cells are first incubated in 100µL of 1° antibodies diluted in FACS staining buffer (1x PBS, 1% fetal bovine serum, 0.09% sodium azide) for 30 minutes on ice. After washing two times with FACS staining buffer, cells are then incubated in 100µL of 2° antibodies diluted in staining buffer on ice for 30 minutes. Cells are washed again with staining buffer, and then fixed for 20 minutes on ice using 4% paraformaldehyde. Cells are washed one final time and resuspended in 300µL of FACS staining buffer and stored at 4°C until analysis. 1° antibodies for NOS2 (Rabbit IgG, SantaCruz) and MMR (Goat IgG, R&D) were diluted at 1:100, while 2° antibodies (PerCP donkey anti-rabbit IgG, Jackson Immunoresearch and PE donkey anti-goat IgG, Jackson Immunoresearch) were diluted at 1:200.

During FACS, the cells are suspended in liquid and flowed through a laser and detector, which can then detect the fluorescent dye of the antibodies. Cells are then separated into individual droplets, which can be charged positively or negatively, and then are run through an electric field, causing positively, negatively, and neutrally charged cells to be separated (Fig.4-6). The number and intensity of cells presenting fluorescent markers is also counted. Data from FACS can be interpreted either as dot plots, which plot each cell as one point with the axes being fluorescent intensities of different wavelengths, or histograms, which plot the number of cells at any given intensity for one wavelength. Expression of the cell markers of interest will result in a higher intensity at the dye's wavelength. FACS is performed on the NOS2 and MMR surface proteins to detect M1 and M2 polarization, respectively.

FACS stained cells were analyzed using the FACSCanto II (BD Biosciences, San Jose, CA), and data analysis was done using both dot plots and histogram plots. Cells cultured without bioactive molecules were used as a negative control. Gating was set so control cells stained positive for approximately 5% of cells for the markers of interest.

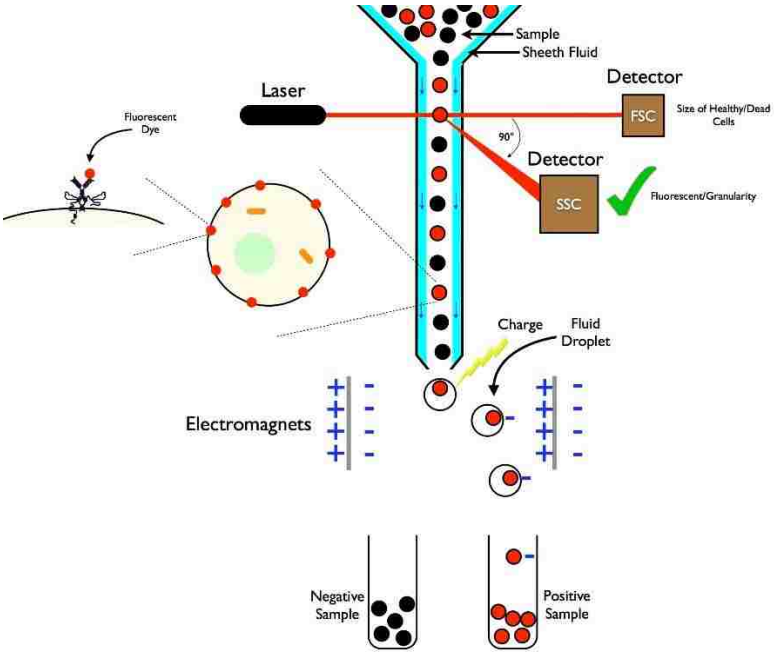

Figure 4-6. Schematic of the FACS procedure (Image from [60], creative commons license).

4.3.5 Enzyme-linked immunosorbent assay (ELISA)

ELISA is a method that is commonly used to detect the presence of antigens [61]. Typically, an antigen is attached to a surface. Then, an antibody specific to the antigen of interest is incubated to the surface, attaching to the antigens. The antibody will have an enzyme attached to it, which can then be detected by optical methods. “Sandwich” ELISA is a method that will have antibodies on the surface attached that are specific to the antigen, allowing other materials that are not of interest to be washed off after the initial incubation. The surface is then incubated again with the antigen specific antibodies that have attached enzymes that can be detected optically (Fig. 4-7). Typically, the optical detection is done in a plate reader, and a standard curve can be created for quantification of the antigen. For our applications, sandwich ELISA will be performed on TNF-α and IL-10 to detect M1 and M2 polarization of macrophages, respectively.

ELISA was performed using Read-Set-Go! ELISA kits (eBioscience, San Diego, CA). High bind 96-well plates (#9018 Costar, Corning Inc., Corning, NY) were first coated with 100μL/well of capture antibody in coating buffer at 4°C overnight. Wells were then washed for 1 minute, three times, with 250μL wash

buffer (1x PBS, 0.05% Tween-20). Wells were then blocked with 200µL of 1x ELISPOT diluent (eBioscience) at room temperature for 1 hour. After washing one time with wash buffer, 100µL of samples were incubated in the wells for 2 hours at room temperature. Standard curve samples were incubated as well, starting at 1000pg/mL, with a 1:2 serial dilution to create an 8-point standard curve. Samples were washed for 1 minute, five times, with wash buffer, after which 100µL of detection antibody was incubated at room temperature for 1 hour. Detection antibody was washed for 1 minute, five times, with wash buffer, and 100µL of Avidin-HRP was incubated in the wells for 30 minutes at room temperature. Wells were then washed for 2 minutes, seven times, before the addition of 100µL of TMB Substrate Solution (eBioscience) for 15 minutes. Finally, 50µL of 1M H_3PO_4 was added as a stop solution. The plate was read immediately at 450nm and 570nm wavelengths in a plate reader. 570nm wavelength values served as a background noise control, and were subtracted from the 450nm wavelength values. Experimental samples were quantified by comparing them to the standard curve samples.

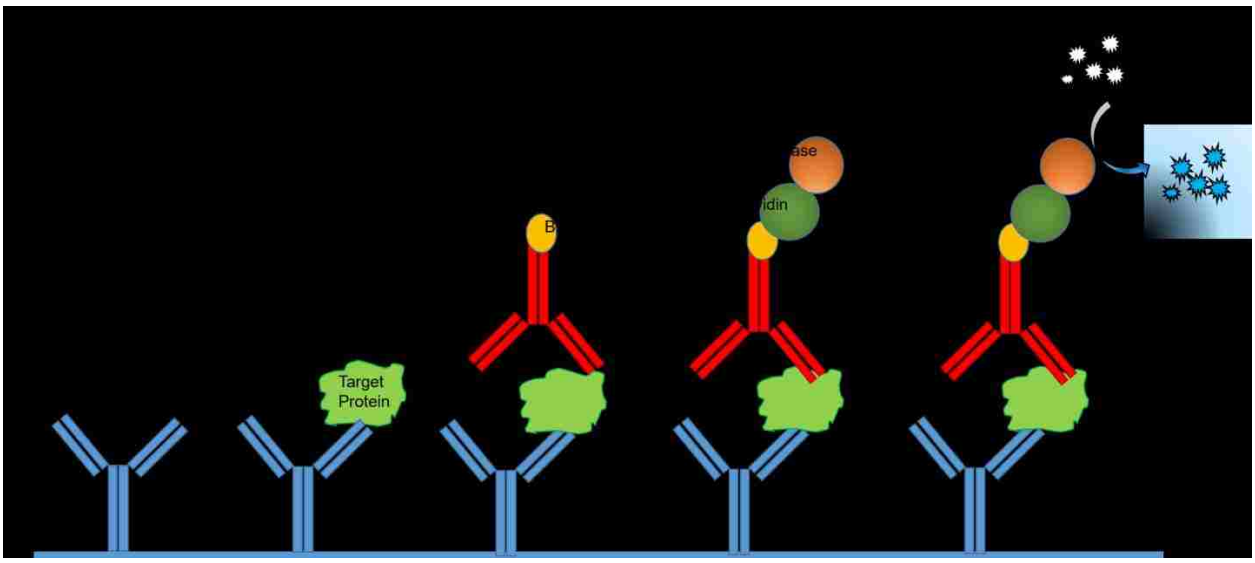

Figure 4-7. Schematic of the sandwich ELISA procedure.

4.3.6 Quantitative real-time polymerase chain reaction (qRT-PCR, or qPCR)

qPCR is a method that allows for the quantitative measurement of DNA levels in a biological sample. For the purposes of our investigation, we are interested in using reverse transcription PCR, which allows for the measurement of RNA levels in a biological sample, which lets us measure the expression of different proteins that we are interested in monitoring.

qPCR uses reporter-quencher marked probes, which fluoresce when the probes hybridize to DNA strands that have their target sequence. The fluorescent signal increases as there are more DNA strands with the target sequence, allowing real time relative quantification of the target sequence (Fig.4-8).

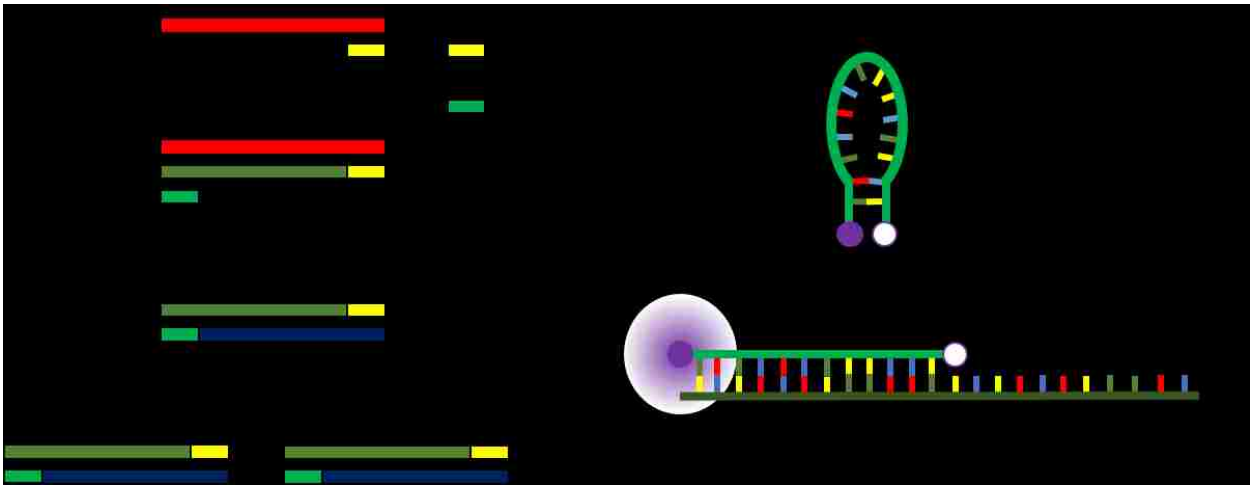

Figure 4-84. Schematic of the PCR process. Taqman PCR utilizes reporter-quencher marked probes, which do not fluoresce when unbound to their target DNA sequences. After binding to their target DNA sequence, the reporter is physically distant from the quencher, allowing it to fluoresce when stimulated by light.

Taqman qPCR was performed on the samples using the ABI Prism 7000. Probes specific to IL-6 and Arg1 (Life Technologies, Carlsbad, CA) were used to detect M1 and M2 polarization, respectively. BMDMs samples were prepared using the Cells-to-Ct 1-Step Taqman kit (Ambion). Culture medium was aspirated and wells were washed with 100μL cold PBS. 49μL of Lysis Solution with 1μL DNase (Ambion) was pipetted up and down 5 times in the wells and incubated at room temperature for 5 minutes. 5μL of Stop Solution (Ambion) was then pipetted up and down 5 times into the lysate and incubated at room temperature for 2 minutes. PCR reaction volume was 10μL, with 2.5μL of Taqman 1-Step qRT-PCR mix, 0.5μL primer-probe, 6μL RNAse free water, and 1μL lysate. Samples were transferred to Semi-skirted PCR plates (T-3085-1, Sorensen Bioscience, Murray, UT) and sealed with a plate sealer. Plates were run in the ABI Prism 7000 by 5 minutes of 50°C for reverse transcription, 20 seconds of 95°C for denaturation, and cycling through 95°C for 15 minutes and 60°C for 1 minute, 40 times, for gene amplification.

4.3.7 Digestion of UBM ECM

Dry sheets of UBM samples were first cut manually with a scalpel or razor blade into small (<1mm square) pieces for pepsin digestion. UBM samples were then digested in a solution of 1mg/mL pepsin in 1% HCl solution, as per the Badylak lab's protocols. [62, 63, 64] Unfortunately, a Waring blender or rotary knife mill was not available for use, so the UBM powder we produced was not uniform in size. UBM digestion proceeded for 48 hours with mixing at room temperature. Pepsin was then inactivated by addition of 1M NaOH until a pH of 7.4 was reached.

4.4 Results

4.4.1 LPS and IL-4 in culture media showed an effect on M1 and M2 polarization via FACS

LPS and IL-4 solubilized in the cell culture media (sLPS and sIL-4, respectively) showed the expected effects on BMDM polarization. sLPS induced M1 polarization of BMDMs, indicated by increased NOS2 expression, while sIL-4 induced M2 polarization, indicated by increased MMR expression (Fig. 4-9).

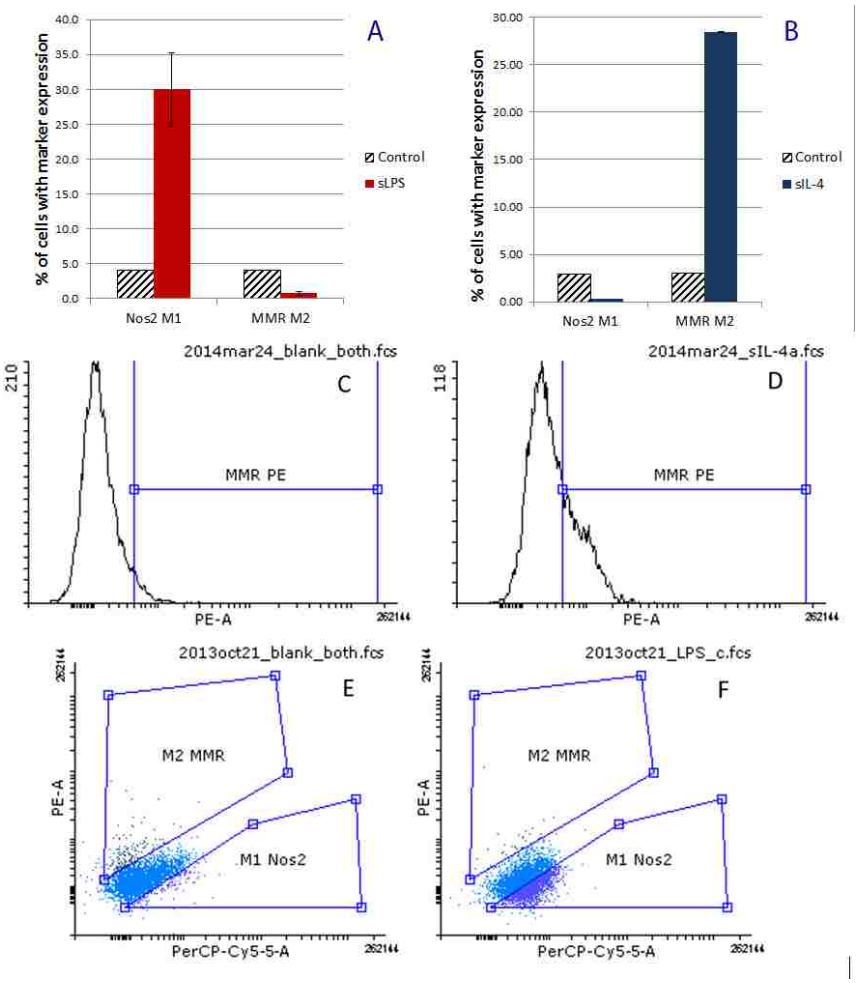

Figure 4-95. Surface marker expression for BMDMs cultured with LPS and IL-4 in solution. A) NOS2 and MMR expression of BMDMs cultured with LPS added to cell culture media. B) NOS2 and MMR expression of BMDMs cultured with IL-4 added to cell culture media. C) and E) FACS plot of control BMDMs cultured without bioactive molecules. D) FACS plot of BMDMs cultured with IL-4 in media F) FACS plot of BMDMs cultured with LPS in media.

4.4.2 FACS analysis of immobilized bioactive molecules

FACS analysis of cells cultured on immobilized IL-4 and immobilized LPS (iIL-4 and iLPS, respectively) was inconclusive. When cells were harvested by gentle scraping during the staining process, much of the plasma deposited pHEMA coating on the glass petri dishes was also scraped off into the cell media. This resulted in a large amount of debris in the FACS readings, which made the data unreliable (Fig. 4-10).

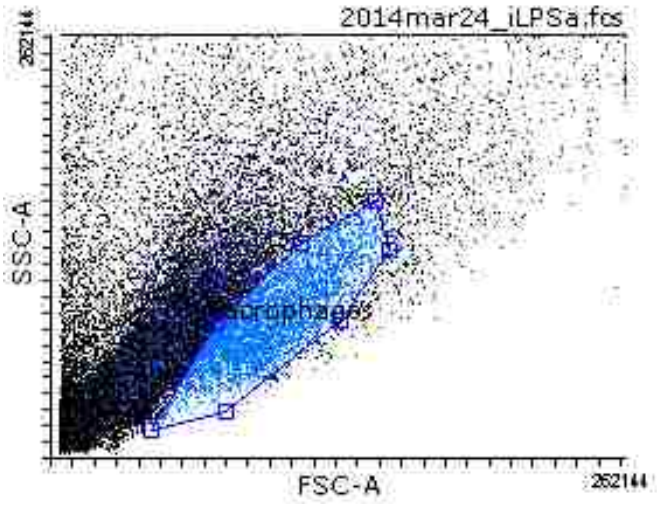

Figure 4-10. Example of unreliable FACS data due to pHEMA debris.

5.4.3 Badylak pep1 and pep2 showed no significant changes in surface marker expression

FACS staining of macrophages cultured with pep1 and pep2 in solution showed these peptides had no effect on macrophage polarization. Because pep1 and pep2 were shown to have chemoattractant effects on macrophages, we expected them to have some influence on the polarization of BMDMs. However, there was no statistically significant difference between the Nos2 and MMR surface expression of BMDMs cultured in regular media compared to BMDMs cultured with pep1 or pep2 (Fig. 4-11).

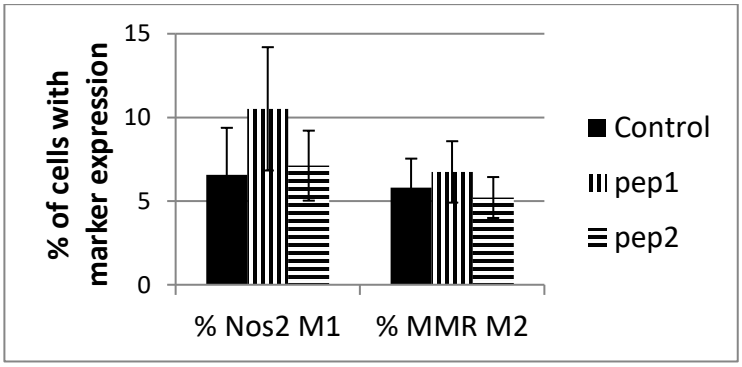

Figure 4-6. BMDMs treated with Badylak peptides in culture medium showed no discernible difference in NOS2 and MMR surface marker expression via FACS analysis, compared to controls.

4.4.4 Cytokine measurements from ELISA of BMDMs cultured with LPS and IL-4 media

We expect to see TNF-α expression and IL-10 expression of BMDMS to be in the picogram to nanogram per mL range [65, 66], and the difference between non-activated and activated BMDM expression to vary

by 10-fold or more. Pilot experiments in ELISA showed significant increases in TNF-α and IL-10 levels for BMDMs cultured with LPS in solution or LPS immobilized on culture surfaces (Fig. 4-12). However, IL-4, both in solution and immobilized, did not show differences of TNF- α or IL-10 levels in the culture media.

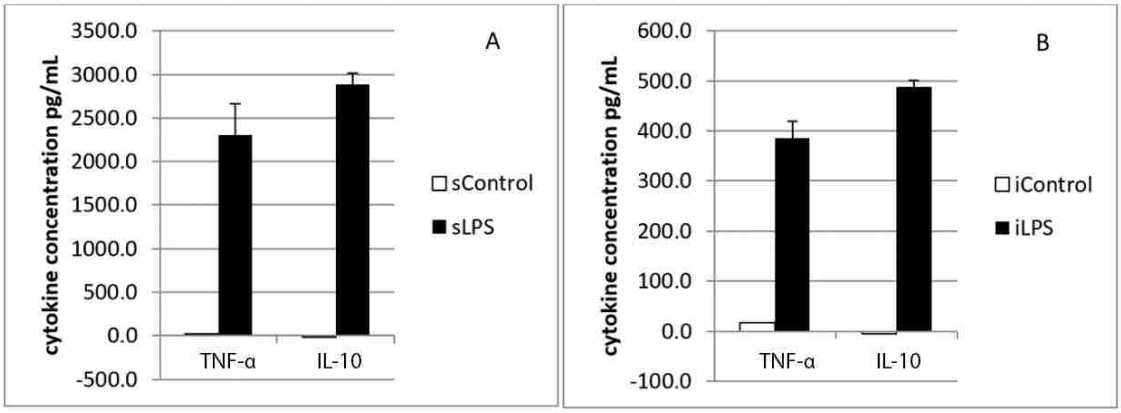

Figure 4-12. A) LPS solubilized in cell culture media resulted in an increase in both TNF-α and IL-10 expression. B) LPS immobilized on the pHEMA coated cell culture surfaces also resulted in an increase in TNF-α and IL-10 expression, although not as greatly as the LPS solubilized in media.

The data presented show that the IL-10 expression levels appeared to be greater than TNF-α levels. This may have been due to the TNF-α optical absorbance in the ELISA readings to be higher than the values in the linear region of the standard curve. This was a result of not knowing the concentrations of cytokines present in the media prior to performing the ELISA; in other assays the samples were diluted to prevent oversaturation of the absorbance readings. We also see that samples with LPS added in solution had much higher TNF-α expression than samples with immobilized LPS. This is expected, as the activity of LPS is expected to be lowered due to the immobilization process. Exact amounts of immobilized LPS were not measured, but is assumed to be lower than that of LPS in solution.

4.4.3 Assessment of M1 response of BMDMs to LPS via a dose response curve

To determine the optimal concentration of LPS to use for further experimentation, a dose response curve of macrophage response was experimentally created (Fig. 4-13). BMDMs cultured on pHEMA coated glass slides were treated with concentrations of LPS varying from 0.01ng/mL to 1000ng/mL. M1 response was measured using ELISA measurements of TNF-α as described above.

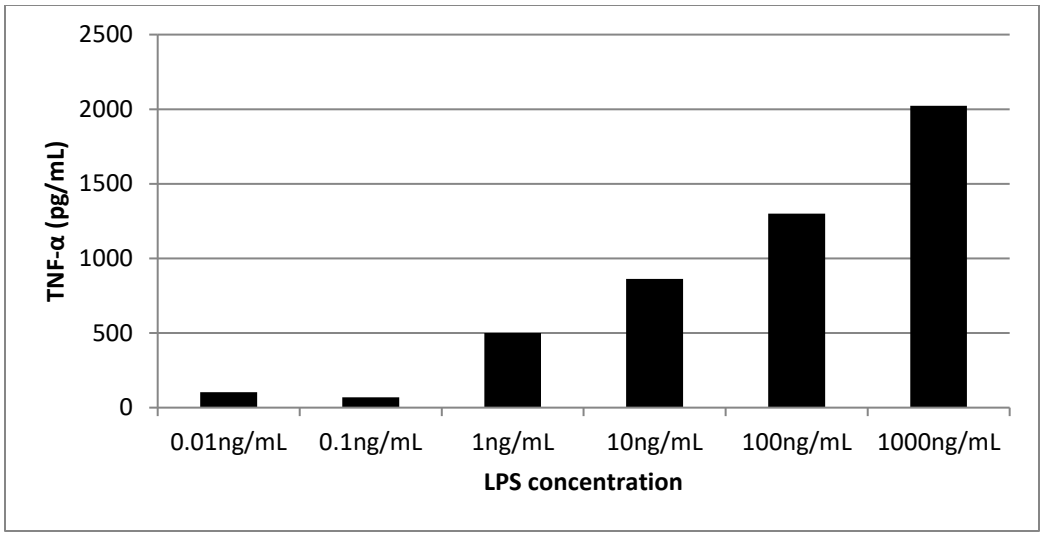

Figure 4-13. LPS dose response curve of BMDMs. TNF-α concentrations measured in culture media of BMDMs 48 hours after addition of LPS. Only 2 samples were used per concentration, so error bars are not shown.

The data in Figure 4-13. suggests that the use of 1ng/mL of LPS for our experiments would be optimal. This concentration provides an easily detectable concentration of TNF-α, which corresponds with M1 polarization. Higher concentrations of LPS were not used, since the effect of soluble or immobilized bioactive molecules may show a small effect in reduction of M1 polarization. High concentrations of LPS may overshadow the effect of M2 promoting conditions, which could possibly result in false negative data.

4.4.4 Cytokine measurements from ELISA of BMDMs cultured with AGP and Col6

ELISA measurements of TNF-α were also performed on BMDMs treated with AGP and Col6 in the solution of culture media (sAGP and sCol6) (Fig. 4-14). These experiments involved the culture of BMDMs with LPS added in solution (1ng/mL) to induce an M1 polarization state. A reduction in TNF-α expression would demonstrate the ability of AGP and Col6 to reduce the M1 state of BMDMs. AGP (112.5 µg/mL) and Col6 (2.5ug/mL) were first introduced in solution to confirm the M1 reducing effect of these bioactive molecules. Immobilized AGP (iAGP) and immobilized Col6 (iCol6) surfaces were also created on 10mm glass discs using plasma deposition and CDI immobilization techniques (as described above). BMDMs were transferred onto modified glass discs, with LPS added to cell culture media after 24

hours. At 48 hours, the culture media was harvested and TNF-α concentrations were measured via ELISA.

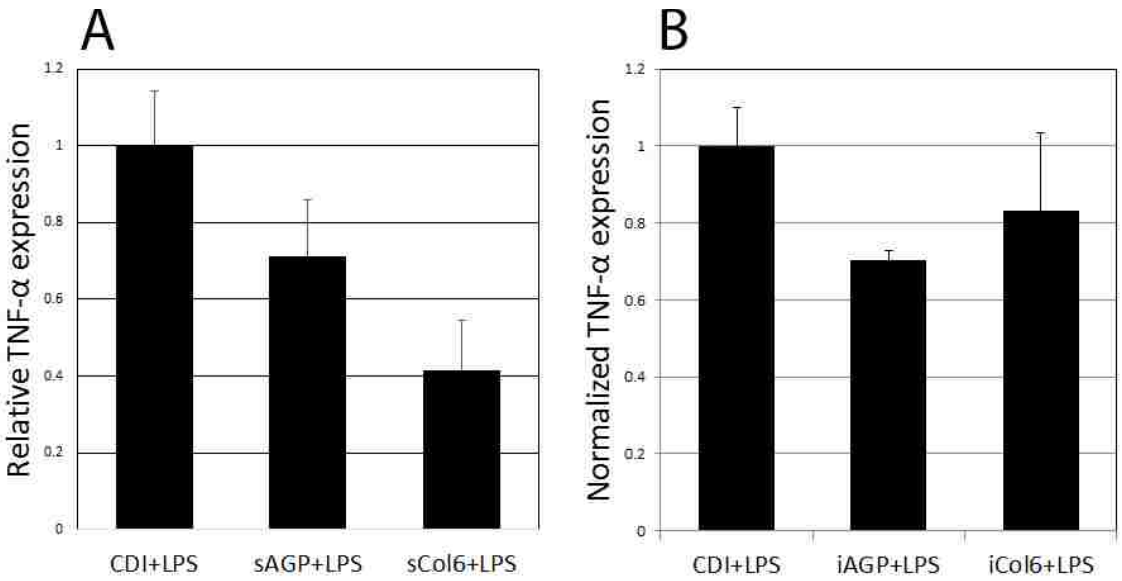

Figure 4-14. Normalized expression of TNF-α measured by ELISA for BMDMs cultured on pHEMA coated glass slides. A) Soluble AGP and Col6 introduced into cell culture media show a large decrease, although highly variable, in TNF-α expression of BMDMs that have been M1 polarized with LPS. B) AGP immobilized onto pHEMA coated glass slides via CDI showed a significant ($p<0.05$) decrease in TNF-α expression of BMDMs that have been M1 polarized with LPS. iCol6 samples showed inconsistent reduction of TNF-α.

TNF-α expression was normalized to that of the control surface (CDI activated pHEMA quenched with deionized water). sAGP and sCol6 showed a large decrease in TNF-α expression, although the measurements were highly variable. iAGP showed a significant ($p<0.05$) decrease in TNF-α expression. iCol6 measurements were highly variable over 4 experiments, ranging between 0.47 and 1.17 expression relative to the control, so these data were not included in the figures.

4.4.5 RT-PCR analysis of the effect of iAGP and iCol6 on Arg1 expression

To assess the effect of immobilized AGP and Col6 on M2 polarization of macrophages, RT-PCR was used to measure the expression of Arg1. BMDMs cultured on iAGP and iCol6 was performed as per the ELISA experiments, except LPS was not added to the culture media at 24 hours. An extra experimental group with AGP and Col6 immobilized onto the same surface was included in these experiments as well.

All experiments were performed with at least n=3. Arg1 expression of experimental groups were calibrated to control BMDMs (cultured on CDI activated pHEMA quenched with deionized water), with GAPDH as an endogenous control (Fig. 4-15).

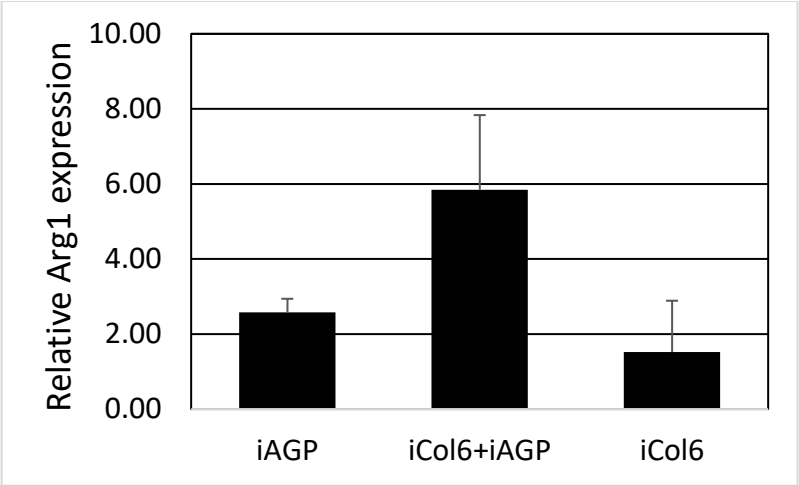

Figure 4-75. RT-PCR measurements of Arg1 expression in BMDMs relative to control. A) iAGP and iCol6+iAGP both showed a statistically significant($p<0.05$) increase in Arg1 expression relative to controls. iCol6 showed highly variable effects on Arg1 expression, varying from a decreased expression to increased expression of Arg1 relative to controls.

BMDMs cultured on iAGP showed a small but significant increase in Arg1 expression, while BMDMs cultured on iCol6 showed a highly variable change in Arg1 expression; some experiments showed a large increase in Arg1 expression, while others showed a decrease in Arg1 expression. These results are what encouraged the use of surfaces with the combination of immobilized Col6 and AGP. BMDMs cultured on iCol6+iAGP showed a larger increase in Arg1 expression than all other experimental groups.

4.4.6 BMDM morphology in relation to polarization

Although M2 polarization is typically assessed using macrophage surface markers or the biological compounds released by macrophages, there is some evidence that a macrophage's morphology also correlates to its polarization. While M1 or resting macrophages typically appear as fibroblast-like cells with more extended processes rather than being elongated, M2 macrophages may appear to be lyphoblast-like with very short processes [67]. A few images were obtained of macrophages cultured on modified surfaces.

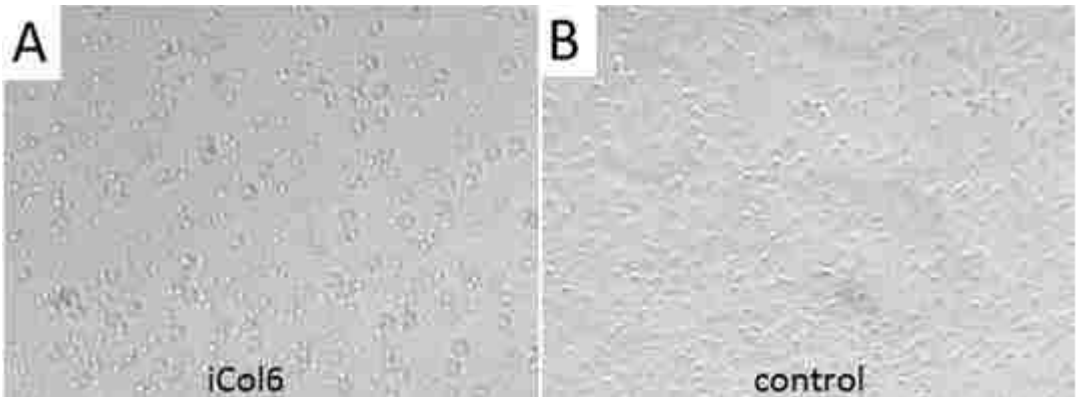

Figure 4-86. M2 macrophages show a different morphology from resting macrophages. A) BMDMs cultured on iCol6 show a morphology similar morphology found in literature, which contrasts with B) BMDMs cultured on pHEMA surfaces activated with CDI.

The morphology of BMDMs cultured on iCol6 showed lymphocyte-like morphology consistent with what is found in literature for M2 macrophages. BMDMs cultured on control surfaces of CDI treated pHEMA, as well as immobilized bovine albumin, showed the same morphology as would be expected from resting macrophages (Fig. 4-16). BMDMs cultured on iAGP did not show the lymphocyte-like morphology that was expected.

4.4.7 RT-PCR analysis of the effect of UBM degradation products on Arg1 expression

Pepsin-digested UBM was also tested in solution or immobilized on BMDMs as described above. Soluble UBM (sUBM) was introduced into the BMDM culture media at 1mg/mL, and immobilized UBM (iUBM) was immobilized with CDI chemistry at 1mg/mL in pH 10.2 buffer.

Trial #	sUBM	iUBM
1	75.58	0.97
2	8.11	0.77
3	2.01	1.08

Table 4-1. Expression of Arg1 in BMDMs treated with UBM relative to control over three experiments.

sUBM degradation products showed large, but inconsistent, increase of Arg1 expression in BMDMs. iUBM showed effectively no effect on Arg1 expression (Table 4-1).

4.5 Discussion

BMDMs were successfully harvested from mice femurs, and grew to maturity in 7 days. These cells were subsequently used to test the M1 and M2 polarizing capabilities of different bioactive molecules. BMDM

cell culture experiments confirmed that LPS and IL-4 in culture media caused M1 and M2 polarization, respectively. This was analyzed using FACS, which showed an increase in NOS2 expression for M1 polarized cells and increased MMR expression for M2 polarized cells.

FACS analysis of BMDMs cultured with Badylak peptides in culture media did not show any increase in NOS2 or MMR surface marker expression. We believe that although these peptides show macrophages chemoattractant properties, they will not activate macrophages into either an M1 or M2 state.

Analysis of cell samples collected from glass slides with plasma deposited pHEMA showed that FACS analysis would not be appropriate for analyzing cells grown on these surfaces. pHEMA coatings resulted in a significant amount of debris after cells were scraped and stained for FACS analysis. BMDMs harvesting using trypsin could not be used for FACS, since trypsin was not able to remove BMDMs from the pHEMA surface even after 10 minutes of incubation at 37°C. Trypsin has also been shown to damage M2 cell surface markers [68], so this method was not pursued further.

ELISA measurements of TNF-α showed a significant increase in cytokine expression due to both immobilized and solubilized LPS. However, IL-4 showed no effect on cytokine expression, in both the solubilized and immobilized state. This leads us to believe that the IL-4 used may have lost bioactivity. IL-4 studies were not pursued due to its high cost and the extensive literature that already exists surrounding it. Experiments with AGP and Col6 introduced into culture media also showed a significant decrease of TNF-α, confirming the ability of these compounds to reduce M1 polarization. Immobilized AGP and Col6 with AGP were also able to decrease TNF-α expression, supporting the hypothesis that AGP and Col6 are able to affect the polarization of macrophage even after immobilization. Immobilized Col6 without AGP showed highly variable results, and was considered unreliable for M2 polarization.

RT-PCR measurements showed a 2.6-fold increase of Arg1 expression in BMDMs cultured on immobilized AGP, and a 5.9-fold increase of Arg1 expression in BMDMs cultured on immobilized

Col6+AGP. BMDMs cultured on immobilized Col6 showed a very inconsistent change in Arg1 expression. These results support the hypothesis that surfaces with immobilized AGP or immobilized Col6+AGP can increase the M2 polarization of macrophages that come into contact with these surfaces. The reason for the inconsistency of immobilized Col6 alone on Arg1 expression is unknown.

BMDM morphology was lymphocyte-like when cultured on iCol6, but remained fibroblast-like when cultured on iAGP, immobilized albumin, or pHEMA controls. This data remains inconclusive, and is not used to confirm M2 polarization since morphology is not a standard technique to assess macrophage polarization. However, we still consider this a significant result worth noting.

Pepsin-digested urinary bladder matrix showed a large effect on Arg1 expression when introduced in solution. This effect, however, was very inconsistent. This may be due to the process in which the UBM was digested; the equipment to create a uniform UBM powder was not available in our lab, resulting in digestion particles that varied greatly in size. Some of the UBM digestion processes may have resulted in the creation of the appropriate peptide sequences for influencing macrophage polarization, while others may have been either cleaved to too small a sequence or were not sufficiently digested to the proper length. Immobilized UBM digestion products did not show any effect on macrophage polarization, which is believed to be because the digestion products need to be internalized by BMDMs to take effect.

Chapter 5: *In vivo* analysis of immobilized bioactive molecules on the foreign body response

5.1 Introduction

Although *in vitro* assays are a powerful tool in determining if immobilized bioactive molecules influence macrophage polarization, *in vivo* experiments need to be performed to see the full effect of immobilized molecules on the FBR. In these experiments, we are interested in seeing the effect of immobilizing M2 promoting molecules onto pHEMA slabs implanted subcutaneously. The foreign body capsule that forms around the implant will be characterized by thickness, density, and vascularity. In addition, staining the implant and surrounding tissue with immunohistochemistry methods to determine the presence of M2 surface markers on macrophages at the implant site will be performed. This data gives insight into the efficacy of immobilized bioactive molecules in affecting the FBR.

5.2 Background

5.2.1 Foreign Body Giant Cells(FBGCs) in the FBR

As mentioned before, FBGCs are believed to play a large role in the FBR. FBGCs begin develop around an implanted material by day 3, and usually become fully formed by day 14. They release many different cytokines that mediate the FBR, including pro-fibrogenic factors, which increase the development of the fibrous capsule. However, some contradicting evidence has shown that reduction of FBGCs number and size present at the FBR site does not reduce the formation of the FBC [69, 70]. This phenomenon implies that the upregulation of FBGC presence at the implant site may not necessarily result in increased FBR and thicker FBC. We believe the analysis of FBGCs at the implant surface may still provide some insight in how our modified surfaces may affect the progression of the FBR.

5.2.2 BALB/c mice

In vivo studies were performed with BALB/c mice to assess the polarization of macrophages at the implant surface. BALB/c mice have been shown to support fully developed M2 activated macrophages [71]. C57/Bl6 mice have shown M2 activated macrophages in adipose tissue [72], which is highly present in the subcutaneous region of mice, so they were not used in these studies. Although previously

performed *in vivo* studies done in our lab, as well as others [73], have shown great variability in FBC thickness when implants are placed subcutaneously, subcutaneous implantation is much less intrusive and harmful to mice. With the proper staining methods, we are able to appropriately analyze the subcutaneous FBR.

5.2.3 Time point for FBR

For our initial experiments, we plan on using the 3 week timepoint for analysis of macrophage polarization and the FBR. Because FBC formation is visible in explants by week 2 [74], we hope to see FBCs by week 3 of implantation. This relatively short time point (compared to many FBR studies done at 7-10 weeks) is preferred to reduce experiment cost and time. The FBC development may also overshadow the effects of our immobilized molecules at later time points, since the length of efficacy of our modified surfaces is unknown.

5.3 Materials and methods

5.3.1 Implant toxicity testing

Cytotoxicity of implants were evaluated by incubating them in Dulbecco's Modified Eagle Medium (DMEM) for 24 hours. The conditioned DMEM was then exposed to NIH-3T3 fibroblast cells for 72 hours. At 24, 48, and 72 hour timepoints, the viability of the fibroblast cells were evaluated by light microscopy and compared to the viability of cells with unconditioned DMEM as well as cells with latex conditioned DMEM. Endotoxicity of implants was evaluated using a standard limulus amebocyte lysate (LAL) assay (Lonza, Basel, Switzerland). Endotoxin levels of below 0.06EU/mL were required for samples to be considered endotoxin free.

5.3.2 Subcutaneous implantation in mice

pHEMA discs of 3 mm diameter and 1 mm thickness were implanted subcutaneously in BALB/c mice. These pHEMA discs had either AGP or Col6+AGP immobilized onto their surfaces as described above. Mice were anesthetized with ketamine-xylazene(130mg/kg-8.8mg/kg) before any surgical procedures.

Bilateral implants (2 impants per mouse) were placed into backside of mice (Fig. 5-1). An incision was made through shaved skin along the spine of the mice. A scalpel blade was used to create a small pocket below the skin for the implant. The skin wound was then closed with surgical clips. Mice were given 0.05mg/kg burprenorphine post-surgery and 8 hours after surgery. The study presented in this document was performed with 8 mice over two trials, with implants identified in Table 5-1. Because of the small sample size, this is considered a pilot study, and the data can only be used to support future experiments rather than draw strong conclusions about the *in vivo* efficacy of the immobilized molecules of interest.

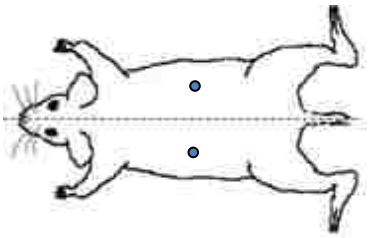

Figure 5-1. Implant locations in mice for subcutaneous implants.

	Mouse ID	Left side	Right side
Trial 1	A0	1 AGP	2 CDI
	A1	3 AGP	4 CDI
	A2	5 Col6+AGP	6 CDI
	A3	7 Col6+AGP	8 CDI
	B0	9 AGP	10 Col6+AGP
Trial 2	A-1	2L AGP	1R AGP
	A-2	4L CDI	3R CDI
	C-2	6L Col6+AGP	5R Col6+AGP

Table 5-1. Sample assignments for implantation into mice

5.3.3 Histological sectioning

At the 3 week timepoint, pHEMA samples and the surrounding tissue were explanted and processed for histological analysis. Explants were fixed in zinc fixative (2.84mM calcium acetate, 22.8mM zinc acetate, and 36.7mM zinc chloride in 0.1M Tris base) overnight at 4°C. After fixing, explants were dehydrated in ethanol and cleared using xylenes before embedding in paraffin. Embedded implants were then be sectioned using a Leica microtome, deparaffinized, and then rehydrated using a graded ethanol series.

5.3.4 Immunohistochemical staining

For immunohistochemical staining, sections were washed in tris buffered saline(TBS), and 3% hydrogen peroxide in TBS will be used to block endogenous peroxidases. To retrieve antigens, sections were incubated in heated(~100°C) 0.1 M pH 6 citrate buffer, and then blocked overnight at 4 ºC in TBS containing 0.5% tween-20, 4% normal serum (Vector Labs, Burlingame, CA) from the animal in which the secondary antibody was raised, and 0.25% immunohistochemical grade bovine serum albumin (BSA) (Vector). Sections were then incubated with diluted primary antibodies for the antigen of interest for 1 hour, and then incubated with a secondary antibody that is selective to the primary antibody for 30 minutes. A Vectastain ABC kit (Vector) was used in conjunction with a diaminobenzidine kit (Vector) to generate a positive brown stain. Counterstaining was not performed, and slides were mounted in Permount.

5.3.5 MECA staining to determine capsule vascularity

The polarization of macrophages in the FBC is believed to determine the tissue remodeling during the FBR, including the vascularization of the FBC and surrounding tissue [75, 76]. Mouse endothelial cell antigen (MECA) was stained using the technique described above. MECA primary antibodies (BD Biosciences) was diluted in a 1:66 ratio, while secondary rabbit anti-rat antibodies (Vector) was diluted in a 1:200 ratio. Staining of MECA can be used to determine the presence of capillaries present in the tissue sections [77]. We analyze the region within 50μm of the implant surface, since we are only interested in capillaries that are part of the FBC [60]. Capillary density was determined using the Weidner method [78]; any stained endothelial cell or endothelial cell cluster that is clearly separate from adjacent vasculature and connective tissue is considered an individual microvessel. This includes vessels that may be "snaking" in and out of the section, appearing as multiple microvessels.

5.3.6 Immunohistochemistry for M1 M2 macrophage markers

Rat anti-F4/80 primary antibodies (BMA Biomedicals, Aust, Switzerland) diluted 1:100 were used as a primary antibody to detect mouse macrophages. Goat anti-macrophage mannose receptor (MMR) (R&D

systems, Minneapolis, MN) diluted 1:100 were used as an M2 marker. MMR is a surface marker highly expressed in macrophages that have undergone M2 polarization, but can also be found in skin cells such as dermal fibroblasts and keratinocytes. MMR+ staining of cells that are believed to be fibroblasts and keratinocytes were ignored for the purposes of this study. Negative controls are rat and goat isotype IgG, respectively. After incubation of sections with primary antibodies, secondary antibodies of biotinylated rabbit anti-goat (1:200, Invitrogen) and biotinylated rabbit anti-rat (1:200, Invitrogen) were used to detect the primary antibodies. Imaging was done under brightfield microscopy to visualize the different markers, and sections were analyzed in the same fashion as MECA stained slides. Instead of counting capillaries, we will count the number of cells staining positive for each marker. No counterstain was used, since other cells and tissues were visible under brightfield microscopy without it.

6.3.7 Trichrome staining for FBC analysis

Trichrome staining was used to assess the FBC. A standard trichrome stain was performed on 6μm thick sections of explants. This stain colors the nuclei of cells black, collagen blue, and cells red. These slides are useful in evaluating the thickness and density of collagen in the FBC, as well as the presence of cells within the FBC.

5.5 Results

5.5.1 Analysis of FBC by trichrome staining

Microtome sectioning of explanted samples and tissue proved to be difficult due to the nature of dehydrated hydrogels such as pHEMA becoming very hard and brittle during the embedding process. Tissues around the implant were often damaged, and due to these difficulties, most stained sections did not provide an intact foreign body capsule for analysis. We were able to produce 2 CDI, 2 AGP, and 2 Col6+AGP stained samples that had minimal damage and were suitable for analysis.

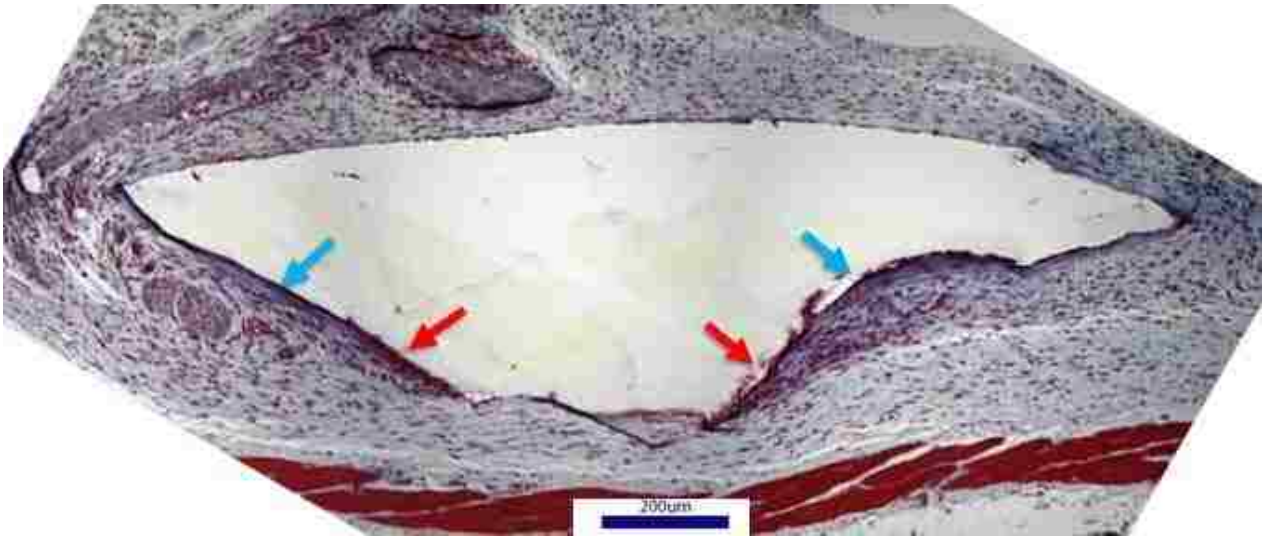

Figure 5-2. Representative trichrome image of the FBC around a CDI control implant (200µm scale bar). Red arrows indicate regions with clusters of red stained cells. Blue arrows indicate regions of densely stained collagen.

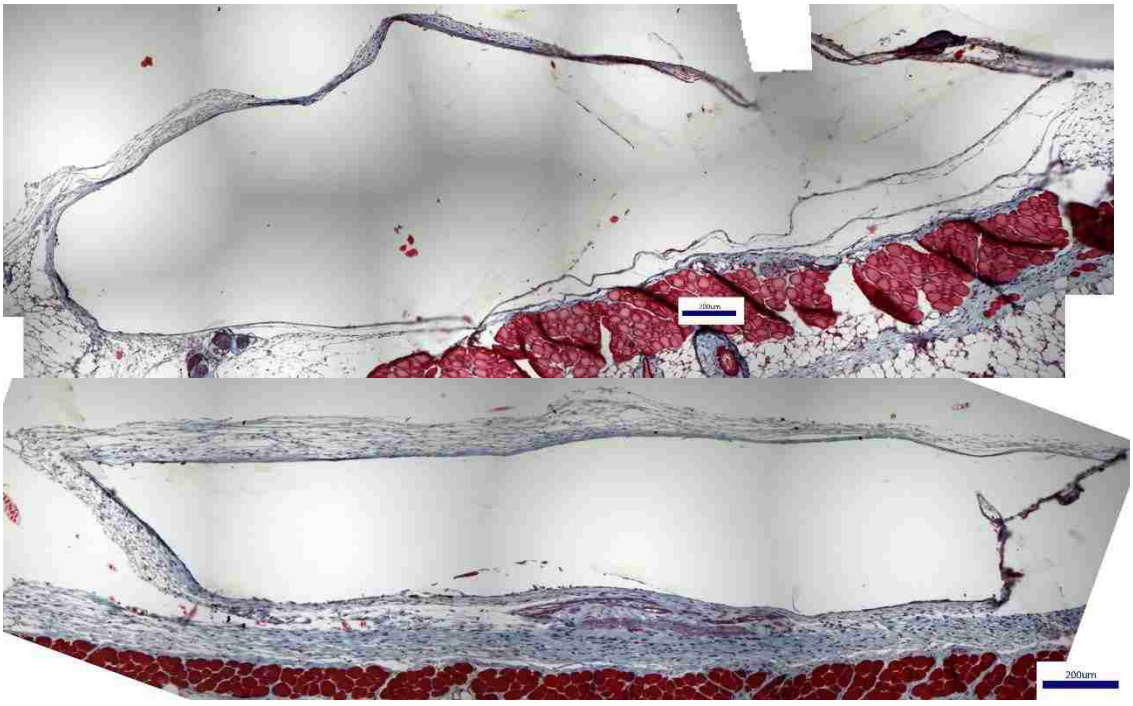

Figure 5-3. Representative images of the FBC around iAGP implants (200µm scale bar).

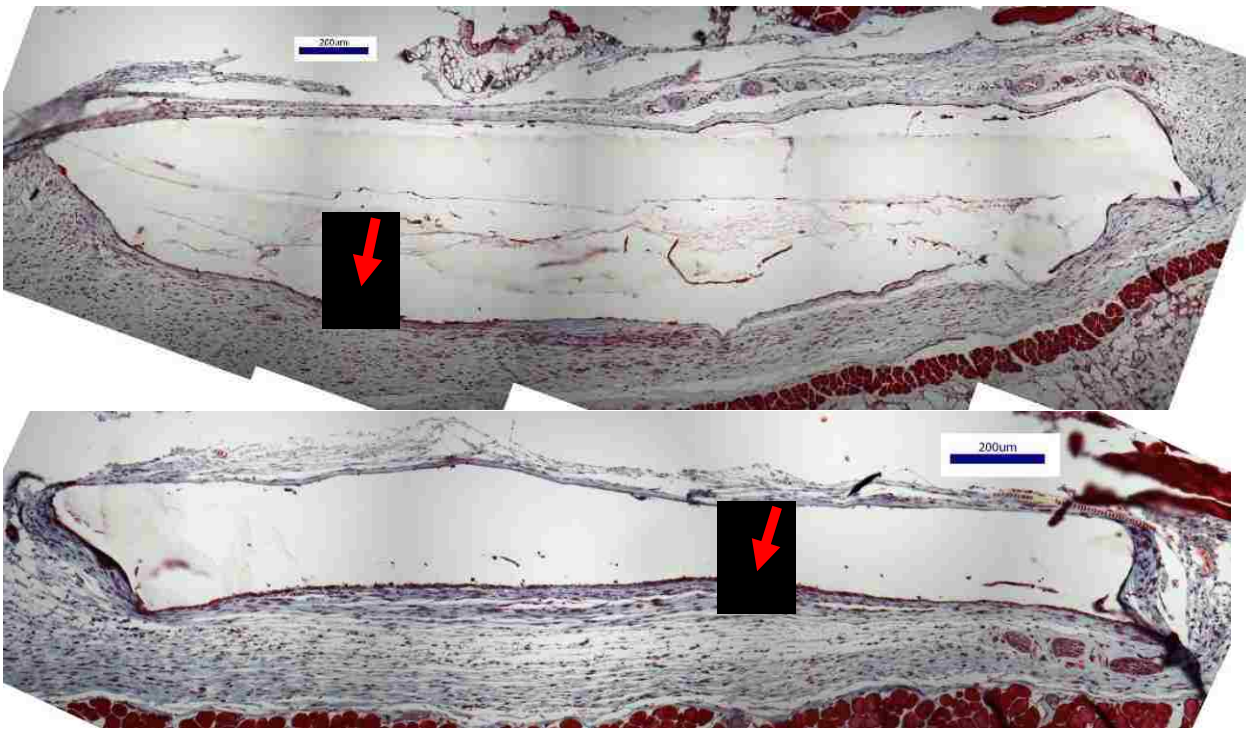

Figure 5-4. Representative images of the FBC around iCol6+iAGP implants (200μm scale bar). Red arrows indicate regions with clusters red stained cells.

A notable difference between the control samples and the samples with immobilized molecules is the presence of large clusters of cells between the FBC and the implant surface (indicated by the red arrows, Fig. 5-2). Although these cell clusters are still present in the iCol6+iAGP samples (Fig. 5-4), they are much thinner. The iAGP samples showed very few of these clusters (Fig. 5-3), and the ones present were very small. We originally believed that these cell clusters may be foreign body giant cells that had formed around the implant. We used the F4/80 stains to test this theory.

Because the FBC has been damaged in processing the samples, thickness measurements would be unreliable. Qualitatively speaking, it appears that the FBC around iAGP samples is thinner and have less dense collagen. We can see regions with darker blue staining (Fig. 5-2, indicated by blue arrows) in the control samples that are not present in the samples. The darker blue stains indicate a higher density of collagen in the region. The iCol6+iAGP samples also appear to have less dense collagen in the FBC, but the thickness does not seem dramatically affected.

5.5.2 Analysis of macrophage presence in the FBC by F4/80 staining

F4/80 stained slides showed numerous macrophages around all implants. A quantitative analysis was done by selecting four 50µm wide x 200µm long regions of the FBC along the implant (Fig. 5-8). Some slides showed severe delamination of the sections from the slide surface, most likely a result of poor adhesion and washing steps during the staining process. This resulted in some samples only being analyzed in 2 or 3 regions, since some delaminated regions were impossible to image properly. To compensate for this, we calculated the average count of macrophages per selected region to do quantitative comparisons.

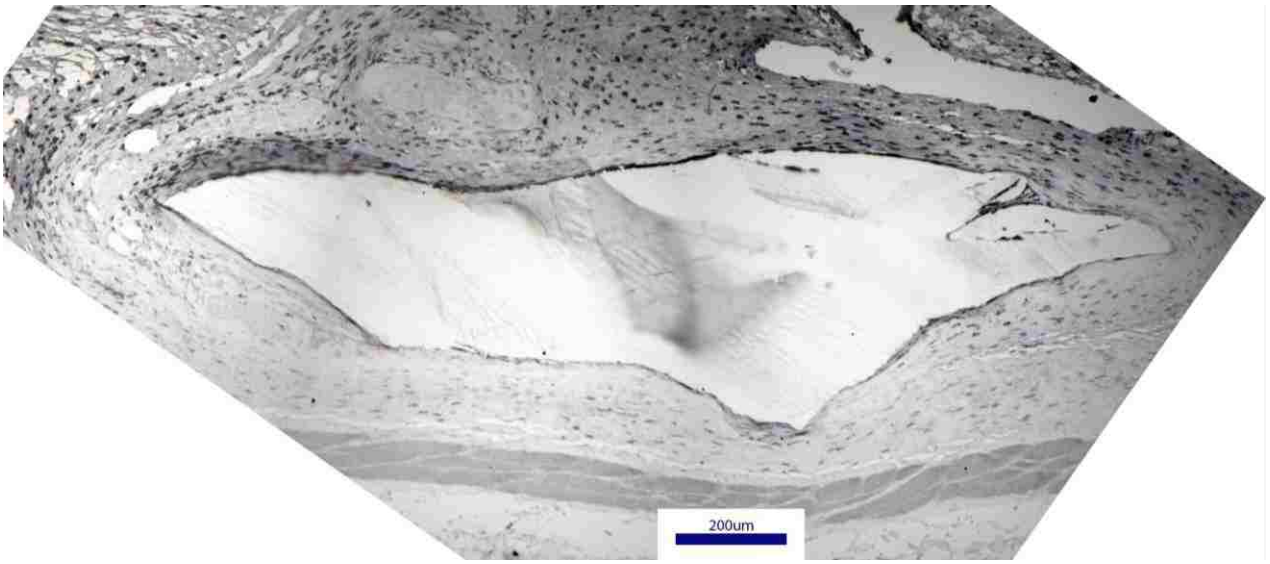

Figure 5-5. Representative image of F4/80 staining of macrophages around a CDI control implant (200µm scale bar).

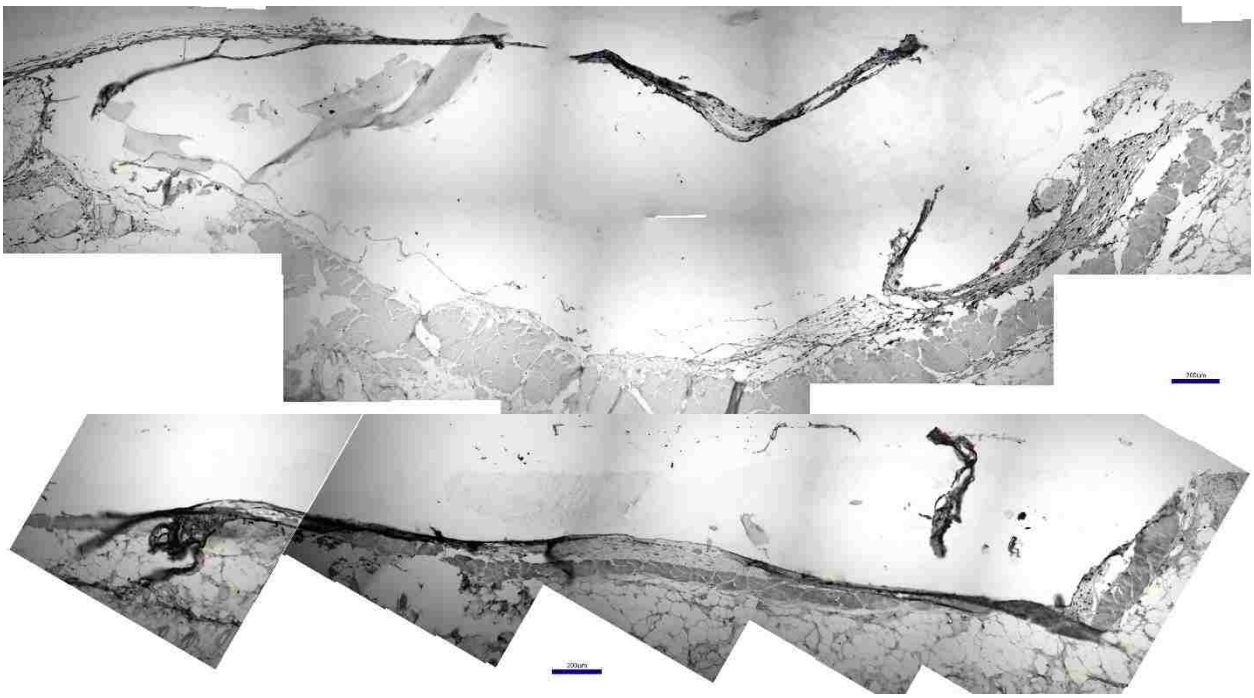

Figure 5-6. Representative images of F4/80 staining of macrophages around iAGP implants (200μm scale bar).

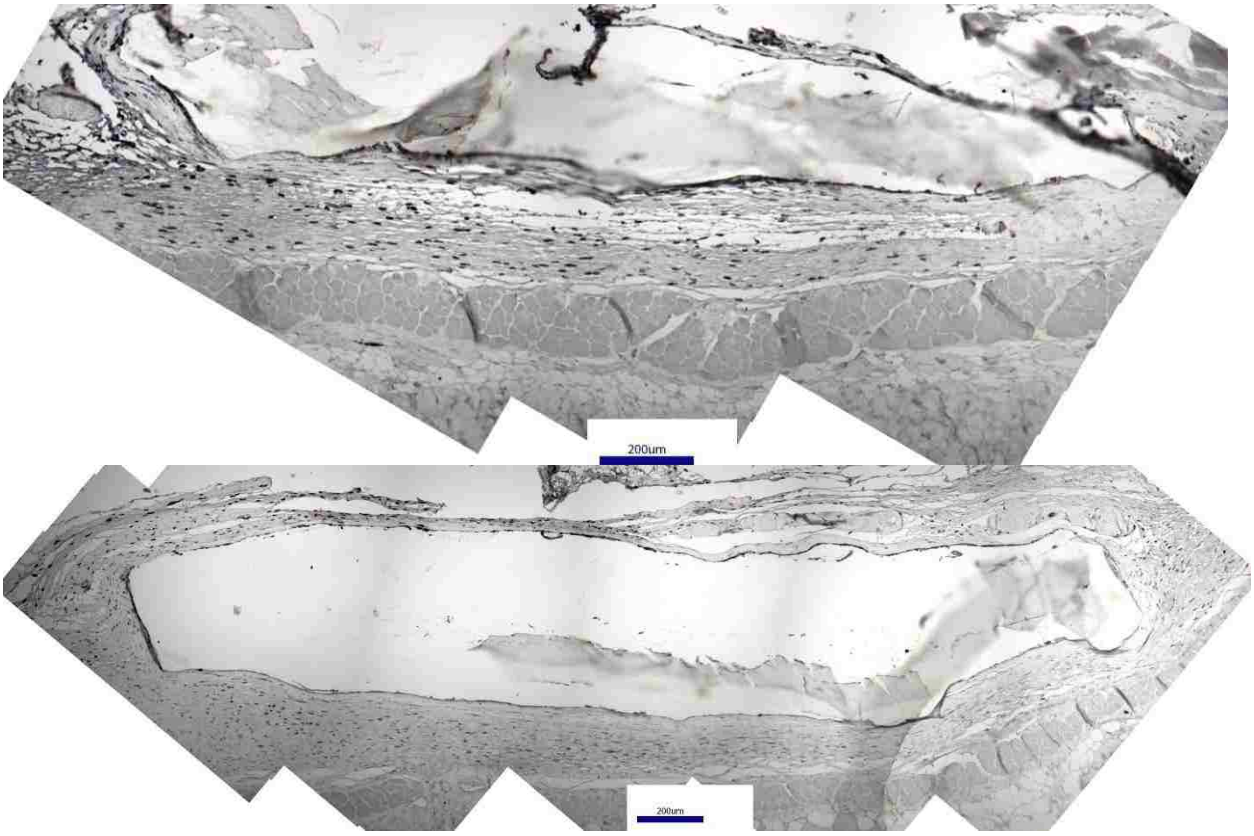

Figure 5-7. Representative images of F4/80 staining of macrophages around iCol6+iAGP implants (200μm scale bar).

The locations of the clusters of red cells in the trichrome stained samples do not appear to correspond to the F4/80 stains of macrophages (Figs. 5-5, 5-6, 5-7). This contradicts the hypothesis that these areas are FBGCs, meaning they may be either fibroblasts or possibly other cells of the immune system.

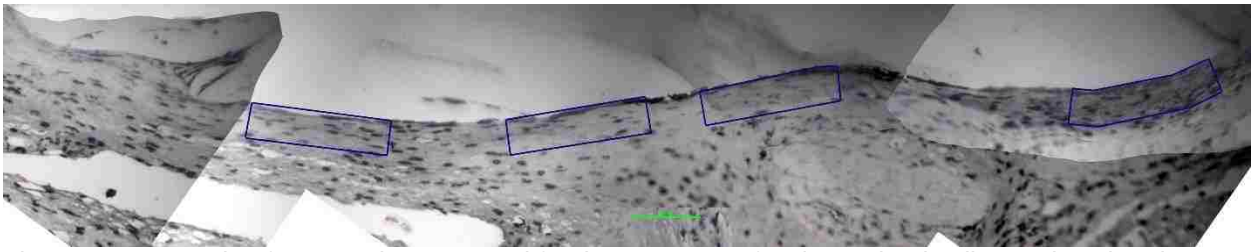

Figure 5-8. Example of FBC regions counted for the presence of F4/80 stained cells. Analyzed regions are shown in the blue rectangles (100μm scale bar).

	Average F4/80+ cells per 0.01mm^2 region
4L iCDI	19.5±5.7
6A2 iCDI	54±14.9
1R iAGP	39.5
2L iAGP	25.5
6L iCol6+iAGP	25±1
7A3 iCol6+iAGP	22.5±5.1

Table 5-2.Average numbers of F4/80 stained cells per section (standard deviation could not be calculated for some samples due to the number of viable regions for counting).

The counts of F4/80 stained cells in each sample did not seem to have any correlation to the sample type (Table 5-2). This leads us to believe that the modified surfaces do not have a measurable chemoattractant effect on macrophages *in vivo*.

5.5.3 Analysis of macrophage polarization in the FBC by MMR staining

The presence of MMR stained macrophages was quantitatively analyzed in the same method as the counting of F4/80 stained cells (Figs. 5-9, 5-10, 5-11). The percentage of macrophages stained MMR+ was then compared across samples by dividing the average number of MMR+ cells per region by the average number of F4/80+ cells per region.

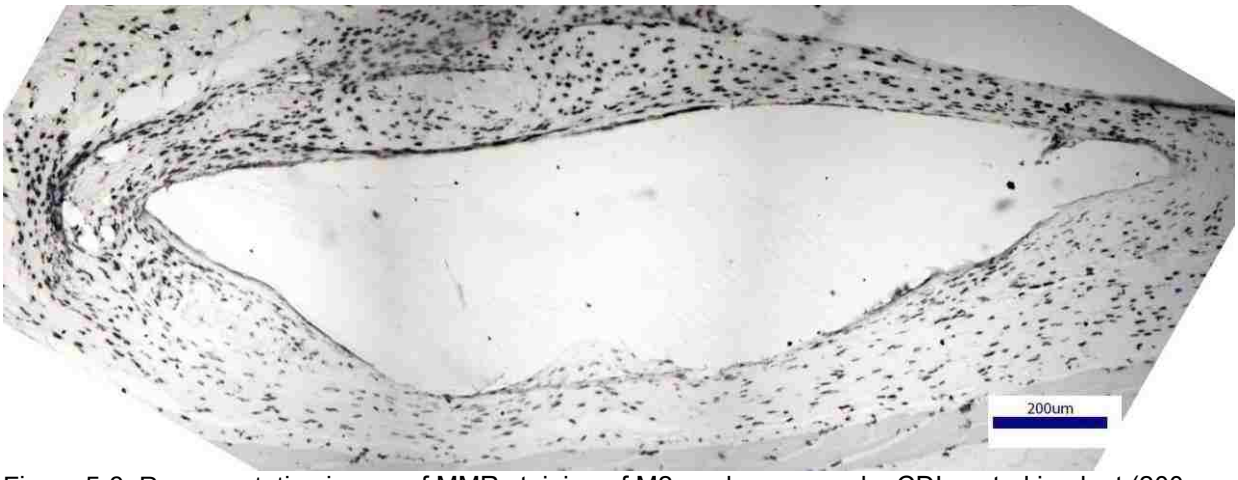

Figure 5-9. Representative image of MMR staining of M2 markers around a CDI control implant (200μm scale bar).

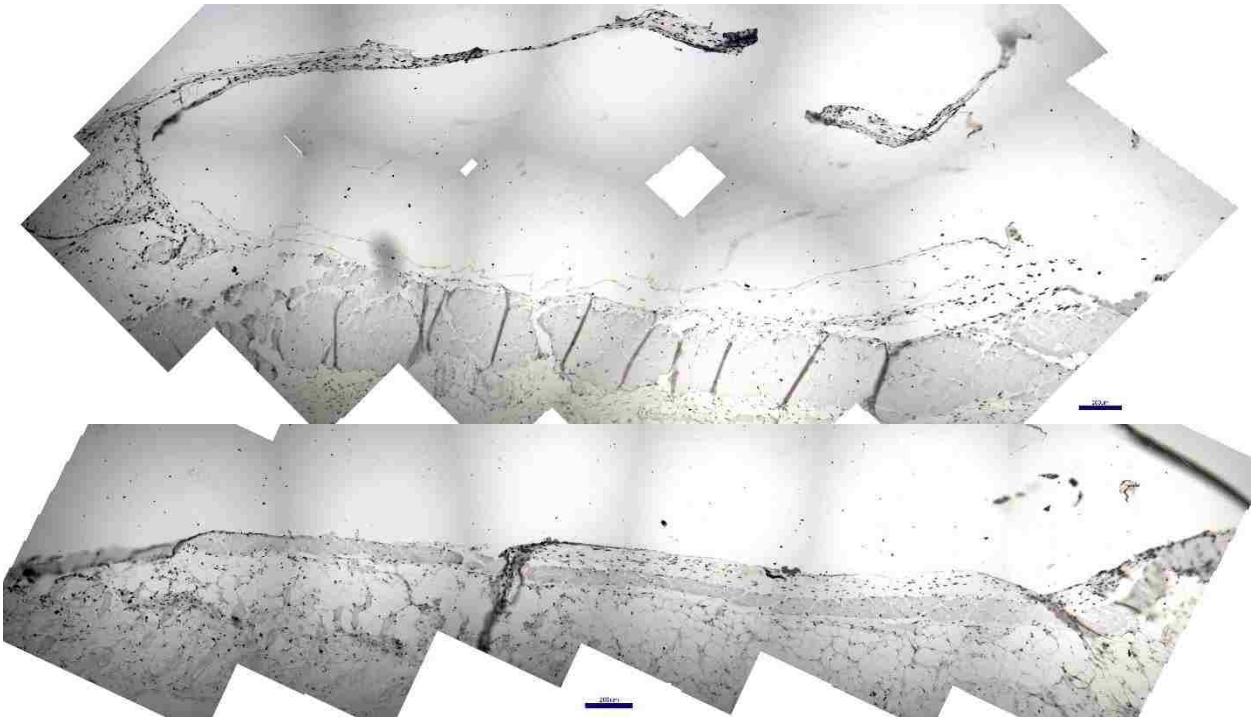

Figure 5-1. Representative images of MMR staining of M2 markers around iAGP implants (200μm scale bar).

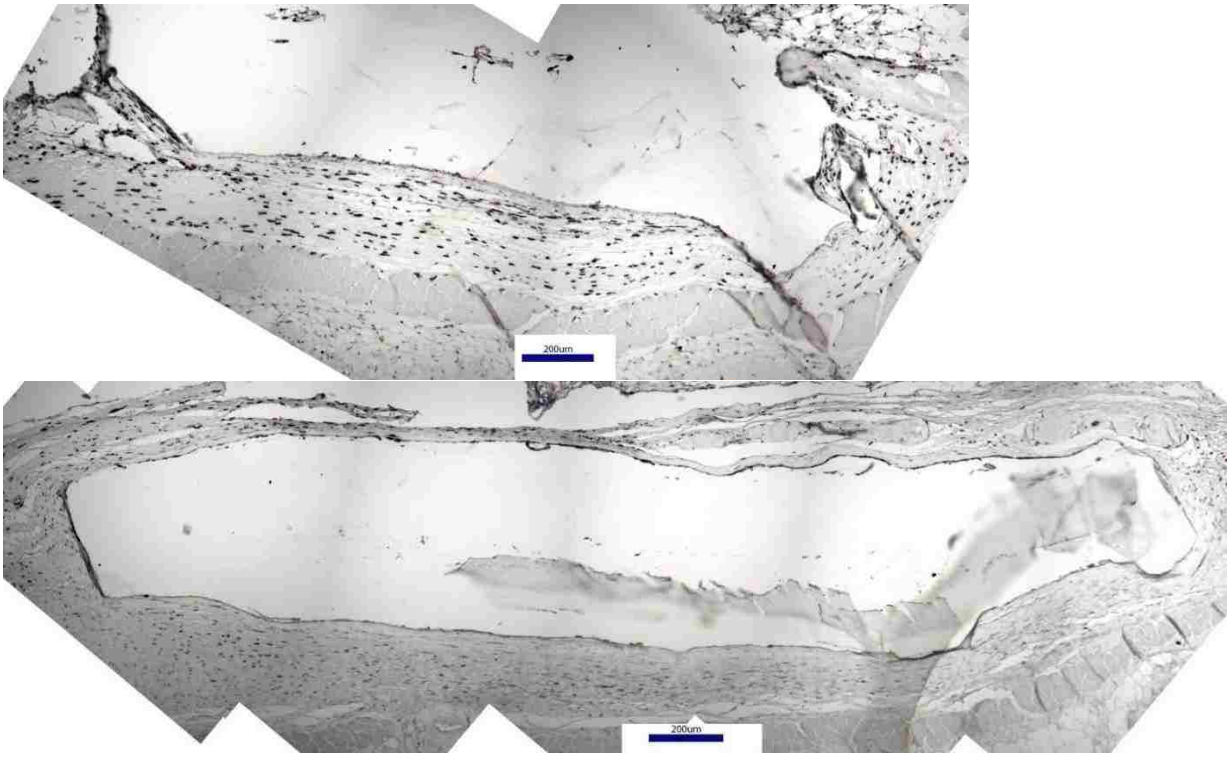

Figure 5-2. Representative images of MMR staining of M2 markers around iCol6+iAGP implants (200μm scale bar).

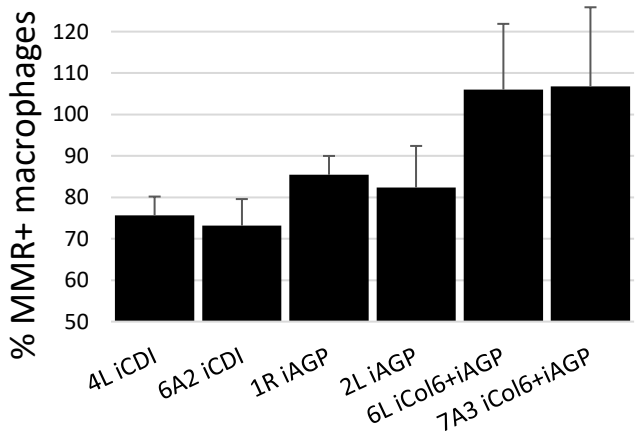

	Average MMR+ cells per region
4L iCDI	14.75±3.1
6A2 iCDI	39.5±7.0
1R iAGP	29±3.6
2L iAGP	21±6.1
6L iCol6+iAGP	26.5±7.9
7A3 iCol6+iAGP	23.5±8.4

Figure 5-3. Percentage of macrophages in the FBC that showed positive staining of the MMR and F4/80 markers (divided by macrophages only showing F4/80 staining). Some samples showed over 100% expression of MMR in stained cells, potentially due to off target staining or variability in cell numbers between sections.

Table 5-3. Average numbers of MMR+ cells per analyzed region.

Comparing the percentage of MMR+ cells suggests that the immobilized molecules influenced the polarization of macrophages at the implant surface. We see a very high percentage of MMR+

macrophages in the iCol6+iAGP samples, and a slightly increased percentage of MMR+ macrophages in the iAGP samples, compared to the CDI controls (Fig 5-12, Table 5-3). Because of our small sample size, we cannot draw any conclusions on statistical significance. However, these pilot data support our hypothesis.

5.5.4 Analysis of capillary formation in the FBC by MECA staining

MECA staining for epithelial cells was also performed on sample sections. Unfortunately, there were too few cells that stained positive for capillary analysis for any quantitative analysis (Fig. 5-13). We can assume that all samples had minimal angiogenesis.

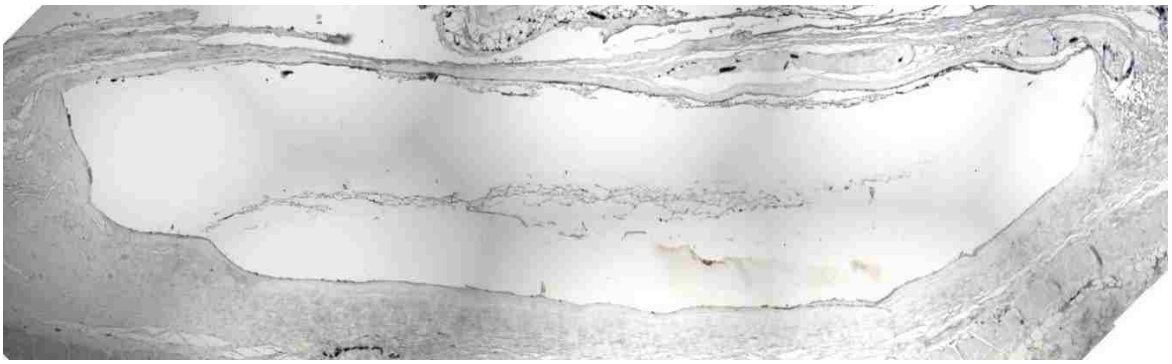

Figure 5-4. Representative image of MECA staining around an iCol6+iAGP implant. All samples had a similar appearance, with very few MECA+ stained cells.

5.5.5 Foreign body giant cells in the FBC around implants

Ideally, the presence of FBGCs in the FBC would be analyzed via scanning electron microscopy, which can confirm their presence via high resolution visualization of cell morphology. However, due to time and money constraints, SEM analysis was not performed. F4/80 stained samples can provide us with an idea of FBGC presence in these samples. We can see that there are many large, elongated F4/80+ cells along the FBC surfaces on all implant types. There do not seem to be any significant differences in size, shape, or number of these large, elongated cells across experimental groups.

5.5.6 Power analysis of pilot study data for future experiments

To determine the number of mice we would need to achieve statistical significance in a future study, we performed power analysis of the MMR+ cell percentages (equations used can be found in the appendix).

The effect size of this statistic in iAGP compared to controls is 1.48, while the effect size iCol6+iAGP is 2.79. This indicates that we will need ~11 mice for the iAGP experimental implant group, and ~6 mice for the iCol6+iAGP group. We would also need 11 mice for the control group, to match that of the iAGP group, for statistical significance.

5.6 Discussion

This pilot study of how immobilized AGP and Col6+AGP affect the foreign body response shows some promising results. The appearance of the foreign body capsule under trichrome stain seems to differ between the control and experimental groups. Control samples showed the presence of large clusters of red cells at the implant surface, and a relatively dark collagen stain. These clusters of cells were not macrophages, confirmed by negative F4/80 staining, and could be fibroblasts or other immune response cells. Fibroblasts could contribute to a denser, less permeable FBC. The lack of these large cell clusters in the experimental groups shows promise in this respect. The lower density of collagen in the FBC of experimental groups also indicates a more permeable capsule, which would be advantageous for several medical applications.

Analysis of MMR stained cells showed trends that support the hypothesis that immobilized AGP or immobilized Col6 in conjunction with AGP can modulate the macrophage response *in vivo*. Although not statistically significant with our small sample size, we saw a slight increase in the percentage of macrophages that stained positive for MMR in iAGP samples, and a large increase in iCol6+iAGP samples. A power analysis of our data indicates that a study with 11 mice for the iAGP group and control group will be needed, while the iCol6+iAGP group will only need 6 mice to confirm our findings.

Chapter 6: Final conclusions and future directions

The immobilization of macrophage polarizing molecules shows promise in reducing the foreign body response. The foreign body response is a major cause of medical device complications, and by reducing it, we believe medical device performance and lifetime can be greatly improved. Molecules such as α-1 acid glycoprotein are inexpensive, and could potentially be used for coatings on medical devices such as contact lenses and glucose sensors to reduce the inflammatory response of the immune system. Collagen VI, while not as inexpensive, has shown great promise in affecting the foreign body response when used in conjunction with α-1 acid glycoprotein as an immobilized surface coating. In contrast with expensive cytokines such as IL-4 and IL-10, which are commonly used to modulate macrophages towards the M2 polarization [79,80,81], these compounds could provide an affordable and long lasting modification of biomaterial surfaces to improve healing and increase the lifetime of implanted medical devices.

Currently, the Ratner lab is also pursuing the computational design of cytokines to increase their stability and their ability to induce the M2 macrophage response. These engineered cytokines could also be immobilized onto biomaterial surfaces to reduce the foreign body response. It is possible that these computational methods could also be used to increase the efficacy and stability of compounds such as α-1 acid glycoprotein and Collagen VI for these purposes. Because our immobilization techniques are nonspecific for the orientation of immobilized bioactive molecules, we could also potentially use computational design to ensure the proper orientation of immobilized of α-1 acid glycoprotein and Collagen VI for maximal effect.

We believe the methods we have developed and tested could have a tremendous impact on the world of implanted medical devices. If used in conjunction with other technologies, such as porous templated scaffolds [82, 83], we could potentially see a dramatic reduction in the foreign body capsule around implanted devices.

Appendix

Peptide sequences:

Badylak Peptide 1	Badylak Peptide 2	Angiotensinogen
IAGVGGEKSGGF	GPVGPSGPPGK	DRVYIHPFHLLVYS

All Amino Acid peaks:

exact mass	species	aminoacid	Abbreviation
44.0500	C2H6N	ALANINE	Ala, A
43.0296	CH3N2	ARGININE	Arg, R
59.0483	CH5N3	ARGININE	Arg, R
70.0657	C4H8N	ARGININE	Arg, R
73.0640	C2H7N3	ARGININE	Arg, R
100.0875	C4H10N3	ARGININE	Arg, R
101.0953	C4H11N3	ARGININE	Arg, R
110.0718	C5H8N3	ARGININE	Arg, R
127.0984	C5H11N4	ARGININE	Arg, R
70.0293	C3H4NO	ASPARAGINE	Asn, N
87.0558	C3H7N2O	ASPARAGINE	Asn, N
88.0399	C3H6NO2	ASPARAGINE	Asn, N
98.0242	C4H4NO2	ASPARAGINE	Asn, N
88.0399	C3H6NO2	ASPARTIC ACID	Asp, D
44.0500	C2H6N	CYSTEINE	Cys, C
76.0220	C2H6NS	CYSTEINE	Cys, C
84.0449	C4H6NO	GLUTAMINE	Glu, Q
28.0187	CH2N	GLYCINE	Gly, G
30.0343	CH4N	GLYCINE	Gly, G
58.0293	C2H4NO	GLYCINE	Gly, G
72.0440	C3H6NO	GLYCINE	Gly, G
85.0402	C3H5N2O	GLYCINE	Gly, G
87.0558	C3H7N2O	GLYCINE	Gly, G
113.0351	C4H5N2O2	GLYCINE	Gly, G
115.0507	C4H7N2O2	GLYCINE	Gly, G
58.0657	C3H8N	GLUTAMIC ACID	Glu, E
81.0453	C4H5N2	HISTIDINE	His, H
82.0531	C4H6N2	HISTIDINE	His, H
95.0609	C5H7N2	HISTIDINE	His, H
110.0718	C5H8N3	HISTIDINE	His, H
121.0402	C6H5N2O	HISTIDINE	His, H
86.0970	C5H12N	ISOLEUCINE	Ile, I
70.0657	C4H8N	LEUCINE	Leu, L
86.0970	C5H12N	LEUCINE	Leu, L
60.0449	C2H6NO	L-SERINE	Ser, S
71.0133	C3H3O2	L-SERINE	Ser, S
57.0578	C3H7N	LYSINE	Lys, K
84.0813	C5H10N	LYSINE	Lys, K
61.0110	C2H5S	METHIONINE	Met, M
104.0534	C4H10NS	METHIONINE	Met, M
117.0370	C5H9OS	METHIONINE	Met, M
120.0813	C8H10N	PHENYLALANINE	Phe, F
132.0575	C9H8O	PHENYLALANINE	Phe, F

68.0500	C4H6N	PROLINE	Pro, P
70.0657	C4H8N	PROLINE	Pro, P
69.0340	C4H5O	THREONINE	Thr, T
74.0610	C3H8NO	THREONINE	Thr, T
130.0657	C9H8N	TRYPTOPHAN	Trp, W
159.0922	C10H11N2	TRYPTOPHAN	Trp, W
170.0606	C11H8NO	TRYPTOPHAN	Trp, W
55.0184	C3H3O	TYROSINE	Tyr, Y
107.0497	C7H7O	TYROSINE	Tyr, Y
136.0760	C8H10NO	TYROSINE	Tyr, Y
72.0813	C4H10N	VALINE	Val, V
83.0469	C5H7O	VALINE	Val, V

IL-4 Sequence:
MGLTSQLLPPLFFLLACAGNFVHGHKCDITLQEIIKTLNSLTEQKTLCTELTVTDIFAASKNTTEKETFCRAA
TVLRQFYSHHEKDTRCLGATAQQFHRHKQLIRFLKRLDRNLWGLAGLNSCPVKEANQSTLENFLERLKTI
MREKYSKCSS

IL-10 mouse sequence:
QYSREDN NCTHFPVGQS HMLLELRTAF SQVKTFFQTK DQLDNILLTD SLMQDFKGYL GCQALSEMIQ
FYLVEVMPQA EKHGPEIKEH LNSLGEKLKT LRMRLRRCHR FLKCENKSKA VEQVKSDFNK
LEDQGVYKAM NEFDIFINCI EAYMMIKMKS

Human Collagen VI sequence:
MRAARALLPLLLQACWTAAQDEPETPRAVAFQDCPVDLFFVLDTSESVALRLKPYGALVDKVKSFTKRFI
DNLRDRYYRCDRNLVWNAGALHYSDEVEIIQGLTRMPGGRDALKSSVDAVKYFGKGTYTDCAIKKGLEQ
LLVGGSHLKENKYLIVVTDGHPLEGYKEPCGGLEDAVNEAKHLGVKVFSVAITPDHLEPRLSIIATDHTYRR
NFTAADWGQSRDAEEAISQTIDTIVDMIKNNVEQVCCSFECQPARGPPGLRGDPGFEGERGKPGLPGEK
GEAGDPGRPGDLGPVGYQGMKGEKGSRGEKGSRGPKGYKGEKGKRGIDGVDGVKGEMGYPGLPGCK
GSPGFDGIQGPPGPKGDPGAFGLKGEKGEPGADGEAGRPGSSGPSGDEGQPGEPGPPGEKGEAGDE
GNPGPDGAPGERGGPGERGPRGTPGTRGPRGDPGEAGPQGDQGREGPVGVPGDPGEAGPIGPKGY
RGDEGPPGSEGARGAPGPAGPPGDPGLMGERGEDGPAGNGTEGFPGFPGYPGNRGAPGINGTKGYP
GLKGDEGEAGDPGDDNNDIAPRGVKGAKGYRGPEGPQGPPGHQGPPGPDECEILDIIMKMCSCCECKC
GPIDLLFVLDSSESIGLQNFEIAKDFVVKVIDRLSRDELVKFEPGQSYAGVVQYSHSQMQEHVSLRSPSIR
NVQELKEAIKSLQWMAGGTFTGEALQYTRDQLLPPSPNNRIALVITDGRSDTQRDTTPLNVLCSPGIQVV
SVGIKDVFDFIPGSDQLNVISCQGLAPSQGRPGLSLVKENYAELLEDAFLKNVTAQICIDKKCPDYTCPITF
SSPADITILLDGSASVGSHNFDTTKRFAKRLAERFLTAGRTDPAHDVRVAVVQYSGTGQQRPERASLQFL
QNYTALASAVDAMDFINDATDVNDALGYVTRFYREASSGAAKKRLLLFSDGNSQGATPAAIEKAVQEAQR
AGIEIFVVVVGRQVNEPHIRVLVTGKTAEYDVAYGESHLFRVPSYQALLRGVFHQTVSRKVALG

Calculations for mean free path λ of electrons in polymers

$$\lambda = \frac{M}{\rho n} E_k / (13.6 \ln(E_k) - 17.6 - \frac{1400}{E_k})$$

For nitrogen in pep1:
M = 1060
E_k = 1083
ρ = 1.14g/mL
n=423 valence electrons (188 electrons from carbons, 65 from nitrogen, 96 from oxygen, 74 from hydrogen
λ = 3.13 nm

Assuming pep1 exists as a sphere with density 1.14g/mL, r of pep1 = 0.678nm, thickness of pep1 monolayer is 1.36nm.

For carbon in pHEMA:
M = 130.14
E_k = 1198
ρ = 1.15 g/mL
n = 52 valence electrons (24 from carbon, 18 from oxygen, 10 from hydrogen)
λ = 3.36 nm

$$\frac{I_B}{I_A} = \lambda_X/\lambda_Y \left(e^{\frac{t_B}{\lambda_X sin\theta}} - 1\right)$$

λ_x is for nitrogen in pep1, and λ_y is for carbon in pHEMA. The S-probe ESCA angle is 55°.

I_B/I_A=(3.13/3.36)*e^(1.36/(3.13*sin(55))-1) = 0.584

Statistical t-test:
The t statistic of the experimental data is then calculated using the formula:

$$t = \frac{\bar{X}_T - \bar{X}_C}{\sqrt{\frac{var_T}{n_T} + \frac{var_C}{n_C}}}$$

where $\bar{X}$ is the sample mean, var is the sample variance, and n is the sample size. T denotes the test or treatment population, and C denotes the control population. The t statistic is looked up in a table of significance, which lists the critical values of t for the sample size and chosen alpha level. If the calculated t statistic is higher than the critical value(p), it can be concluded that there is statistical significance in the results, and the null hypothesis can be rejected. Typically, a p of 0.05 is used.

Power analysis calculations:
The effect size of a characteristic is calculated by:

$$\Delta = \frac{|\mu_T - \mu_C|}{\sigma}$$

where Δ is the effect size, μ is the mean of the characteristic for the test(T) and control(C) groups, and σ is the standard deviation for the characteristic. To calculate the number of animals per group (m) in the full study, we use the equation[3]:

$$m = \frac{2\left(z_{1-\frac{\alpha}{2}} + z_{1-\beta}\right)^2}{\Delta} + \frac{z_{1-\frac{\alpha}{2}}^2}{4}$$

where $z_{1-\frac{\alpha}{2}}$ is the standard score for a two tailed t-test of alpha level α, and $z_{1-\beta}$ is the standard score for a power level of β.

References

1 Paul C Nicolson and Jürgen Vogt, “Soft Contact Lens Polymers: An Evolution,” *Biomaterials* 22, no. 24 (2001): 3273–3283.
2 Jeanine K Suchecki, Peter Donshik, and William H Ehlers, “Contact Lens Complications.,” *Ophthalmology Clinics of North America* 16, no. 3 (2003): 471–484.
3 Gary N Foulks, “Prolonging Contact Lens Wear and Making Contact Lens Wear Safer,” *American Journal of Ophthalmology* 141, no. 2 (2006): 369–373.
4 David M Mosser and Justin P Edwards, “Exploring the Full Spectrum of Macrophage Activation,” *Nature Reviews Immunology* 8, no. 12 (2008): 958–969.
5 Alberto Mantovani et al., “The Chemokine System in Diverse Forms of Macrophage Activation and Polarization,” *Trends in Immunology* 25, no. 12 (2004): 677–686.
6 Alberto Mantovani et al., “Macrophage Polarization: Tumor-Associated Macrophages as a Paradigm for Polarized M2 Mononuclear Phagocytes,” *Trends in Immunology* 23, no. 11 (2002): 549–555.
7 James M Anderson, Analiz Rodriguez, and David T Chang, “Foreign Body Reaction to Biomaterials,” in *Seminars in Immunology*, vol. 20 (Elsevier, 2008), 86–100.
8 Yoshinori Onuki et al., “A Review of the Biocompatibility of Implantable Devices: Current Challenges to Overcome Foreign Body Response,” *Journal of Diabetes Science and Technology* 2, no. 6 (2008): 1003–1015.
9 K Sutherland et al., “Degradation of Biomaterials by Phagocyte-Derived Oxidants.,” *Journal of Clinical Investigation* 92, no. 5 (1993): 2360.
10 Brien A Holden and George W Mertz, “Critical Oxygen Levels to Avoid Corneal Edema for Daily and Extended Wear Contact Lenses.,” *Investigative Ophthalmology & Visual Science* 25, no. 10 (1984): 1161–1167.
11 Winterton, Lynn, Silicone Hydrogel Contact Lenses, US 2008/0174035, filed 2007, issued 2008.
12 Ludwik Leibler, “Theory of Microphase Separation in Block Copolymers,” *Macromolecules* 13, no. 6 (1980): 1602–1617.
13 G Young et al., “The Effect of Soft Contact Lens Care Products on Lens Modulus,” *Contact Lens and Anterior Eye* 33, no. 5 (2010): 210–214.
14 Buddy D Ratner, Ashutosh Chilkoti, and Gabriel P Lopez, “Plasma Deposition and Treatment for Biomaterial Applications,” *Plasma Deposition, Treatment and Etching of Polymers*, 1990, 463–516.
15 Wenxi Huang et al., “Functionalization of Surfaces by Water-Accelerated Atom-Transfer Radical Polymerization of Hydroxyethyl Methacrylate and Subsequent Derivatization,” *Macromolecules* 35, no. 4 (2002): 1175–1179.
16 Amir P Ameen et al., “A High-Resolution X-Ray Photoelectron Spectroscopy Study of Trifluoroacetic Anhydride Labelling of Hydroxyl Groups: Demonstration of the B Shift Due To -OC (O) CF 3,” *Polymer* 34, no. 9 (1993): 1795–1799.
17 GS Bethell et al., “A Novel Method of Activation of Cross-Linked Agaroses with 1, 1’-carbonyldiimidazole Which Gives a Matrix for Affinity Chromatography Devoid of Additional Charged Groups.,” *Journal of Biological Chemistry* 254, no. 8 (1979): 2572–2574.
18 Julia Morales-Sanfrutos et al., “Vinyl Sulfone: A Versatile Function for Simple Bioconjugation and Immobilization,” *Organic & Biomolecular Chemistry* 8, no. 3 (2010): 667–675.
19 Vincent Payet et al., “Cleaning of Albumin-Contaminated Ti and Cr Surfaces: An XPS and QCM Study,” *Surface and Interface Analysis* 40, no. 3–4 (March 1, 2008): 215–19, doi:10.1002/sia.2655.
20 MJB Wissink et al., “Immobilization of Heparin to EDC/NHS-Crosslinked Collagen. Characterization and in Vitro Evaluation,” *Biomaterials* 22, no. 2 (2001): 151–163.
21 John F Watts and John Wolstenholme, “An Introduction to Surface Analysis by XPS and AES,” *An Introduction to Surface Analysis by XPS and AES, by John F. Watts, John Wolstenholme, Pp. 224. ISBN 0-470-84713-1. Wiley-VCH, May 2003.* 1 (2003).
22 John C Vickerman and David Briggs, *ToF-SIMS: Materials Analysis by Mass Spectrometry 2nd Edition* (IM publications, 2013).

23 Ashutosh Chilkoti et al., “Analysis of Polymer Surfaces by SIMS. 16. Investigation of Surface Crosslinking in Polymer Gels of 2-Hydroxyethyl Methacrylate,” *Macromolecules* 26, no. 18 (August 1, 1993): 4825–32, doi:10.1021/ma00070a016.
24 Joseph D Andrade, *Surface and Interfacial Aspects of Biomedical Polymers*, vol. 2 (Plenum Press New York, 1985).
25 Yehouda Harpaz, Mark Gerstein, and Cyrus Chothia, “Volume Changes on Protein Folding,” *Structure* 2, no. 7 (1994): 641–649.
26 Kara L. Spiller et al., “Differential Gene Expression in Human, Murine, and Cell Line-Derived Macrophages upon Polarization,” *Experimental Cell Research* 347, no. 1 (September 10, 2016): 1–13, doi:10.1016/j.yexcr.2015.10.017.
27 Manfred Kopf et al., “Disruption of the Murine IL-4 Gene Blocks Th2 Cytokine Responses,” 1993.
28 Jannet T Huang et al., “Interleukin-4-Dependent Production of PPAR-γ Ligands in Macrophages by 12/15-Lipoxygenase,” *Nature* 400, no. 6742 (1999): 378–382.
29 Michael Stein et al., “Interleukin 4 Potently Enhances Murine Macrophage Mannose Receptor Activity: A Marker of Alternative Immunologic Macrophage Activation.,” *The Journal of Experimental Medicine* 176, no. 1 (1992): 4.
30 Audrey Varin and Siamon Gordon, “Alternative Activation of Macrophages: Immune Function and Cellular Biology,” *Immunobiology* 214, no. 7 (2009): 630–641.
31 Jean-Pierre Galizzi et al., “Internalization of Human Interleukin 4 and Transient down-Regulation of Its Receptor in the CD23-Inducible Jijoye Cells.,” *Journal of Biological Chemistry* 264, no. 12 (1989): 6984–6989.
32 Han Ping Shi et al., “The Role of iNOS in Wound Healing,” *Surgery* 130, no. 2 (2001): 225–229.
33 Hartmut Kleinert et al., “Regulation of the Expression of Inducible Nitric Oxide Synthase,” *European Journal of Pharmacology* 500, no. 1 (2004): 255–266.
34 Eeva Moilanen et al., “Nitric Oxide Synthase Is Expressed in Human Macrophages during Foreign Body Inflammation.,” *The American Journal of Pathology* 150, no. 3 (1997): 881.
35 Kang Li et al., “Differential Macrophage Polarization in Male and Female BALB/c Mice Infected with Coxsackievirus B3 Defines Susceptibility to Viral Myocarditis,” *Circulation Research* 105, no. 4 (2009): 353–364.
36 Justin Sturge et al., “Mannose Receptor Regulation of Macrophage Cell Migration,” *Journal of Leukocyte Biology* 82, no. 3 (2007): 585–593.
37 V Apostolopoulos and Mckenzie Ifc, “Role of the Mannose Receptor in the Immune Response,” *Current Molecular Medicine* 1, no. 4 (2001): 469–474.
38 Chiung-I. Chang, James C. Liao, and Lih Kuo, “Arginase Modulates Nitric Oxide Production in Activated Macrophages,” *American Journal of Physiology - Heart and Circulatory Physiology* 274, no. 1 (January 1, 1998): H342–48.
39 Linda D Hazlett et al., “IL-33 Shifts Macrophage Polarization, Promoting Resistance against Pseudomonas Aeruginosa Keratitis,” *Investigative Ophthalmology & Visual Science* 51, no. 3 (2010): 1524–1532.
40 Toby Lawrence and Gioacchino Natoli, “Transcriptional Regulation of Macrophage Polarization: Enabling Diversity with Identity,” *Nature Reviews Immunology* 11, no. 11 (November 2011): 750–61, doi:10.1038/nri3088.
41 Joan K Riley et al., “Interleukin-10 Receptor Signaling through the JAK-STAT Pathway REQUIREMENT FOR TWO DISTINCT RECEPTOR-DERIVED SIGNALS FOR ANTI-INFLAMMATORY ACTION,” *Journal of Biological Chemistry* 274, no. 23 (1999): 16513–16521.
42 Paul P Tak, Gary S Firestein, and others, “NF-κB: A Key Role in Inflammatory Diseases,” *Journal of Clinical Investigation* 107, no. 1 (2001): 7–11.
43 Rene de Waal Malefyt et al., “Interleukin 10 (IL-10) Inhibits Cytokine Synthesis by Human Monocytes: An Autoregulatory Role of IL-10 Produced by Monocytes.,” *The Journal of Experimental Medicine* 174, no. 5 (1991): 1209–1220.

44 ALAN Sher et al., “Production of IL-10 by CD4+ T Lymphocytes Correlates with down-Regulation of Th1 Cytokine Synthesis in Helminth Infection.,” *The Journal of Immunology* 147, no. 8 (1991): 2713–2716.
45 Xinyuan Li et al., “IL-35 Is a Novel Responsive Anti-Inflammatory Cytokine—a New System of Categorizing Anti-Inflammatory Cytokines,” *PloS One* 7, no. 3 (2012): e33628.
46 Bryan N Brown et al., “Macrophage Polarization: An Opportunity for Improved Outcomes in Biomaterials and Regenerative Medicine,” *Biomaterials* 33, no. 15 (2012): 3792–3802.
47 Sherry H-Y Wei et al., “Proteasome-Mediated Proteolysis of the Interleukin-10 Receptor Is Important for Signal Downregulation,” *Journal of Interferon & Cytokine Research* 26, no. 5 (2006): 281–290.
48 Raymond P. Donnelly, Harold Dickensheets, and David S. Finbloom, “The Interleukin-10 Signal Transduction Pathway and Regulation of Gene Expression in Mononuclear Phagocytes,” *Journal of Interferon & Cytokine Research* 19, no. 6 (June 1, 1999): 563–73, doi:10.1089/107999099313695.
49 Daniel J Van Antwerp et al., “Suppression of TNF-α-Induced Apoptosis by NF-κB,” *Science* 274, no. 5288 (1996): 787–789.
50 Nan Ma et al., “Cytotoxic Reaction and TNF-Alpha Response of Macrophages to Polyurethane Particles.,” *Journal of Biomaterials Science. Polymer Edition* 13, no. 3 (2002): 257–72.
51 Thierry Fournier, Najet Medjoubi-N, and Dominique Porquet, “Alpha-1-Acid Glycoprotein,” *Biochimica et Biophysica Acta (BBA) - Protein Structure and Molecular Enzymology* 1482, no. 1–2 (October 18, 2000): 157–71, doi:10.1016/S0167-4838(00)00153-9.
52 Hisakazu Komori et al., “α1-Acid Glycoprotein Up-Regulates CD163 via TLR4/CD14 Protein Pathway POSSIBLE PROTECTION AGAINST HEMOLYSIS-INDUCED OXIDATIVE STRESS,” *Journal of Biological Chemistry* 287, no. 36 (August 31, 2012): 30688–700, doi:10.1074/jbc.M112.353771.
53 Peter D. Yurchenco, *Extracellular Matrix Assembly and Structure* (Academic Press, 2013).
54 Peiwen Chen et al., “Collagen VI Regulates Peripheral Nerve Regeneration by Modulating Macrophage Recruitment and Polarization,” *Acta Neuropathologica* 129, no. 1 (November 25, 2014): 97–113, doi:10.1007/s00401-014-1369-9.
55 Christian R. H. Raetz and Chris Whitfield, “Lipopolysaccharide Endotoxins,” *Annual Review of Biochemistry* 71 (2002): 635–700, doi:10.1146/annurev.biochem.71.110601.135414.
56 Bruce Alberts et al., “Cell Junctions, Cell Adhesion, and the Extracellular Matrix,” 2002, https://www-ncbi-nlm-nih-gov.offcampus.lib.washington.edu/books/NBK21047/.
57 Vineet Agrawal et al., “Recruitment of Progenitor Cells by an Extracellular Matrix Cryptic Peptide in a Mouse Model of Digit Amputation,” *Tissue Engineering Part A* 17, no. 19–20 (2011): 2435–2443.
58 K. Inaba et al., “Generation of Large Numbers of Dendritic Cells from Mouse Bone Marrow Cultures Supplemented with Granulocyte/macrophage Colony-Stimulating Factor.,” *Journal of Experimental Medicine* 176, no. 6 (December 1, 1992): 1693–1702, doi:10.1084/jem.176.6.1693.
59 WA Bonner et al., “Fluorescence Activated Cell Sorting,” *Review of Scientific Instruments* 43, no. 3 (2003): 404–409.
60 SariSabban, *English: Fluorescence Assisted Cell Sorting (FACS) Showing Positive Cell Selection.*, September 1, 2011, Sabban, Sari (2011) Development of an in vitro model system for studying the interaction of Equus caballus IgE with its high- affinity FcεRI receptor (PhD thesis), The University of Sheffield
61 Eva Engvall and Peter Perlmann, “Enzyme-Linked Immunosorbent Assay, ELISA III. Quantitation of Specific Antibodies by Enzyme-Labeled Anti-Immunoglobulin in Antigen-Coated Tubes,” *The Journal of Immunology* 109, no. 1 (1972): 129–135.
62 Stephen Badylak et al., “Small Intestinal Submucosa as a Large Diameter Vascular Graft in the Dog,” *Journal of Surgical Research* 47, no. 1 (July 1, 1989): 74–80, doi:10.1016/0022-4804(89)90050-4.
63 Donald O. Freytes et al., “Preparation and Rheological Characterization of a Gel Form of the Porcine Urinary Bladder Matrix,” *Biomaterials* 29, no. 11 (April 2008): 1630–37, doi:10.1016/j.biomaterials.2007.12.014.

64 Thomas W. Gilbert et al., “Production and Characterization of ECM Powder: Implications for Tissue Engineering Applications,” *Biomaterials* 26, no. 12 (April 2005): 1431–35, doi:10.1016/j.biomaterials.2004.04.042.
65 Koichi S Kobayashi et al., “Nod2-Dependent Regulation of Innate and Adaptive Immunity in the Intestinal Tract,” *Science* 307, no. 5710 (2005): 731–734.
66 Nora E Paul et al., “Topographical Control of Human Macrophages by a Regularly Microstructured Polyvinylidene Fluoride Surface,” *Biomaterials* 29, no. 30 (2008): 4056–4064.
67 Raymond A. Isidro et al., “The Probiotic Mixture VSL#3 Alters the Morphology and Secretion Profile of Both Polarized and Unpolarized Human Macrophages in a Polarization-Dependent Manner,” *Journal of Clinical & Cellular Immunology* 5, no. 3 (June 20, 2014): 1000227, doi:10.4172/2155-9899.1000227.
68 Shaodong Chen et al., “Impact of Detachment Methods on M2 Macrophage Phenotype and Function,” *Journal of Immunological Methods* 426 (November 2015): 56–61, doi:10.1016/j.jim.2015.08.001.
69 Themis R Kyriakides et al., “The CC Chemokine Ligand, CCL2/MCP1, Participates in Macrophage Fusion and Foreign Body Giant Cell Formation,” *Am. J. of Pathology* 165, no. 6 (2004): 2157–2166.
70 T Iizuka, T Kohgo, and SC Marks Jr, “Foreign Body Giant Cell Induction in the CSF-1-Deficient Osteopetrotic (Op/op) Mouse,” *Tissue and Cell* 34, no. 2 (2002): 103–108.
71 De’Broski R Herbert et al., “Alternative Macrophage Activation Is Essential for Survival during Schistosomiasis and Downmodulates T Helper 1 Responses and Immunopathology,” *Immunity* 20, no. 5 (2004): 623–635.
72 Carey N Lumeng et al., “Obesity Induces a Phenotypic Switch in Adipose Tissue Macrophage Polarization,” *Journal of Clinical Investigation* 117, no. 1 (2007): 175–184.
73 W Kenneth Ward et al., “The Effect of Microgeometry, Implant Thickness and Polyurethane Chemistry on the Foreign Body Response to Subcutaneous Implants,” *Biomaterials* 23, (2002): 4185–4192.
74 Ilse MSL Khouw et al., “The Foreign Body Reaction to a Biodegradable Biomaterial Differs between Rats and Mice,” *Journal of Biomedical Materials Research* 52, no. 3 (2000): 439–446.
75 Kara L. Spiller, Donald O. Freytes, and Gordana Vunjak-Novakovic, “Macrophages Modulate Engineered Human Tissues for Enhanced Vascularization and Healing,” *Annals of Biomedical Engineering* 43, no. 3 (March 1, 2015): 616–27, doi:10.1007/s10439-014-1156-8.
76 Kara L Spiller et al., “The Role of Macrophage Phenotype in Vascularization of Tissue Engineering Scaffolds,” *Biomaterials* 35, no. 15 (2014): 4477–4488.
77 Fan Yang et al., “Genetic Engineering of Human Stem Cells for Enhanced Angiogenesis Using Biodegradable Polymeric Nanoparticles,” *Proceedings of the National Academy of Sciences* 107, no. 8 (2010): 3317–3322.
78 Noel Weidner, “Current Pathologic Methods for Measuring Intratumoral Microvessel Density within Breast Carcinoma and Other Solid Tumors,” *Breast Cancer Research and Treatment* 36, no. 2 (1995): 169–180.
79 Kara L. Spiller and Gordana Vunjak-Novakovic, “Clinical Translation of Controlled Protein Delivery Systems for Tissue Engineering,” *Drug Delivery and Translational Research* 5, no. 2 (April 1, 2015): 101–15, doi:10.1007/s13346-013-0135-1.
80 Kara L. Spiller et al., “Sequential Delivery of Immunomodulatory Cytokines to Facilitate the M1-to-M2 Transition of Macrophages and Enhance Vascularization of Bone Scaffolds,” *Biomaterials* 37 (January 2015): 194–207, doi:10.1016/j.biomaterials.2014.10.017.
81 Andrew R. D. Reeves et al., “Controlled Release of Cytokines Using Silk-Biomaterials for Macrophage Polarization,” *Biomaterials* 73 (December 2015): 272–83, doi:10.1016/j.biomaterials.2015.09.027.
82 Eric M. Sussman et al., “Porous Implants Modulate Healing and Induce Shifts in Local Macrophage Polarization in the Foreign Body Reaction,” *Annals of Biomedical Engineering* 42, no. 7 (July 2014): 1508–16, doi:10.1007/s10439-013-0933-0.
83 Robert A. Underwood et al., “Quantifying the Effect of Pore Size and Surface Treatment on Epidermal Incorporation into Percutaneously Implanted Sphere-Templated Porous Biomaterials in Mice,” *J. of Biomedical Materials Research Part A* 98A, no. 4 (September 15, 2011): 499–508, doi:10.1002/jbm.a.33125.